The Arabidopsis active demethylase ROS1 *cis*-regulates immune-responsive genes by pruning DNA methylation at promoter-regulatory regions

Thierry Halter, Jingyu Wang, Delase Amesefe, Emmanuelle Lastrucci, Magali Charvin, Meenu Singla Rastogi and Lionel Navarro☯

Institut de Biologie de l'Ecole Normale Supérieure (IBENS), Centre National de la Recherche Scientifique UMR8197, Institut National de la Santé et de la Recherche Médicale U1024, Paris, France

☯Correspondance : lionel.navarro@ens.psl.eu

Competing interests : the authors declare that no competing interests exist.

HIGHLIGHTS:

- The *TNL RMG1* that is regulated by ROS1 positively regulates basal resistance towards *Pto* DC3000
- ROS1 regulates the flg22-triggered differential expression of more than 2000 thousands genes, among which 10% are demethylated by ROS1
- ROS1 facilitates the transcriptional activation of a subset of flg22-induced genes by antagonizing RdDM at discrete promoter regions
- WRKY transcription factors (TFs) bind to the demethylated promoter regions of a subset of flg22-induced ROS1 targets
- The hypermethylation at the *RLP43* promoter, caused by the lack of ROS1, repels DNA binding of two PAMP-responsive WRKY TFs
- Specific hypermethylation at the ROS1-targeted promoter regions of *RMG1* and *RLP43* is causal for their silencing as well as for disease susceptibility against *Pto* DC3000

Abstract

Active DNA demethylation has emerged as an important regulatory process of plant and mammalian immunity. However, very little is known about the mechanisms by which active demethylation controls transcriptional immune reprogramming and disease resistance. Here, we first show that the Arabidopsis active demethylase ROS1 promotes basal resistance towards *Pseudomonas syringae* by antagonizing RNA-directed DNA methylation (RdDM). Furthermore, we found that ROS1 facilitates the flagellin-triggered induction of the disease resistance gene *RMG1* by limiting RdDM at the 3' boundary of a remnant RC/Helitron transposable element (TE) embedded in its promoter. We further identify flagellin-responsive ROS1 putative primary targets, and show that at a subset of promoters, ROS1 erases methylation at discrete regions exhibiting WRKY transcription factors (TFs) binding. In particular, we demonstrate that ROS1 removes methylation at the orphan immune receptor *RLP43* promoter, to ensure DNA binding of WRKY TFs. Finally, we show that ROS1-directed demethylation of the *RMG1* and *RLP43* promoters is causal for both flagellin responsiveness of these genes and for basal resistance. Overall, these findings significantly advance our understanding of how active demethylases shape transcriptional immune reprogramming to enable antibacterial resistance.

Introduction

Plants are permanently exposed to microbes including pathogens and rely on a potent immune response to control infections. The first layer of the plant immune system involves the recognition of Pathogen- or Microbe- Associated Molecular Patterns (PAMPs or MAMPs), which are sensed by surface-localized Pattern-Recognition Receptors (PRRs) (Couto and Zipfel, 2016). Plant PRRs are composed of Receptor-Like Kinases (RLKs) and Receptor-Like Proteins (RLPs), which are structurally and functionally analogous to animal Toll-Like Receptors (TLRs) (Boutrot and Zipfel, 2017). Flagellin Sensing 2 (FLS2) is a well-characterized surface receptor, which recognizes a conserved 22 amino acid epitope from the N-terminal part of the bacterial flagellin, named flg22 (Boller and Felix, 2009). Upon ligand binding, FLS2 initiates a complex phosphorylation cascade at the PRR complex that leads to early signalling events, which include production of reactive oxygen species (ROS), activation of mitogen-activated-protein-kinases (MAPKs) and differential expression of thousands of genes, which are in part regulated by WRKY transcription factors (TFs) (Navarro et al., 2004, Zipfel et al., 2004, Birkenbihl et al., 2017). To enable disease, pathogens secrete effectors that suppress PTI. For instance, the Gram-negative hemibiotrophic pathogenic bacterium *Pseudomonas syringae* pv. *tomato* strain DC3000 (*Pto* DC3000) injects 36 type-III effectors into plant cells to dampen PTI (Wei et al., 2015). Plants have evolved disease resistance (R) proteins that can perceive the presence of pathogen effectors and trigger a host counter-counter defence (Monteiro and Nishimura, 2018). Most R proteins belong to the nucleotide binding domain (NBD), leucine-rich repeat (NLR) superfamily, which are also present in animals (Jones et al., 2016). Plant NLRs contain N-terminal coiled-coild (CC) or Toll-interleukine (TIR) domain, a central nucleotide-binding site domain (NBS), and C-terminal leucine-rich repeats (LRRs) and are thus referred to as CNLs or TNLs, respectively (Monteiro and Nishimura, 2018). These immune receptors can sense, directly or indirectly, pathogen effectors and mount Effector-Triggered Immunity (ETI), a potent immune response that significantly overlaps with PTI, although with a stronger amplitude (Jones et al., 2016; Thomma et al., 2011). However, very little is known about the functional relevance of *NLRs* in PTI and/or basal resistance towards phytopathogens (Roth et al., 2017).

Rapid and robust activation of plant immune responses are crucial to limit the spread and multiplication of phytopathogens. On the other hand, their sustained induction often leads to cell death and developmental defects. For instance, the constitutive expression of *NLRs* often triggers ectopic cell death (Oldroyd & Staskawicz., 1998; Zhang et al., 2004., Swiderski et al., 2009; Bernoux et al., 2011., Nishimura et al., 2017). A tight control of both plant immune receptors and downstream signalling factors is therefore crucial and involves multi-layered transcriptional, post-transcriptional and post-translational regulatory mechanisms (Van Wersch et al., 2020; Halter and Navarro 2015; Deleris et al., 2016). The transcriptional control of defence genes by DNA methylation and demethylation has emerged as a central regulatory process of the plant immune system (Lopez et al., 2011, Yu et al., 2013; Dowen et al., 2012; Lopez Sanchez et al., 2016; Le et al., 2014; Deleris et al., 2016., Kong et al., 2020).

DNA methylation is an epigenetic mark that negatively regulates the transcription and transposition of transposable elements (TEs). It can also trigger transcriptional silencing of genes carrying TEs/repeats in their vicinity (Matzke and Mosher, 2014). Homeostasis of DNA methylation relies on the equilibrium between methylation and active demethylation pathways, and has been extensively studied in *Arabidopsis thaliana*. In this model organism, DNA methylation is established by the RNA-directed DNA methylation (RdDM) pathway, which is directed by short interfering RNAs (siRNAs) (Matzke and Mosher, 2014). These siRNAs are mainly produced from PolIV-dependent RNAs (P4RNAs) that are converted into double-stranded RNAs (dsRNAs) by RNA-DEPENDENT RNA POLYMERASE2 (RDR2) (Matzke and Mosher, 2014; Blevins et al., 2015; Zhai et al 2015; Yang et al., 2016). The resulted dsRNAs are predominantly processed by DICER-LIKE 3 (DCL3) into 23-24 siRNAs, but additionally, in some instances, by DCL2 and DCL4 into 22 nt and 21 nt siRNAs, respectively; which are all competent for RdDM (Xie et al., 2004; Matzke and Mosher, 2014; Panda et al., 2020). These siRNAs further direct ARGONAUTE 4 (AGO4) to TEs/repeats through base pairing with transcripts generated by Pol V (Zilberman., 2004; Chan et al., 2004; Qi et al., 2006; Wierzbicki et al., 2009). AGO4 then binds to DNA targets and recruits the *de novo* methyltransferase DOMAIN REARRANGED METHYLTRANSFERASE 2 (DRM2) that catalyses methylation in all cytosine sequence contexts (CG, CHG and CHH, where H is any nucleotide but not G) (Cao and Jacobsen., 2002; Cao et al., 2003; Lahmy

et al., 2016). During DNA replication, symmetric CG and CHG methylation are maintained by METHYLTRANSFERASE1 (MET1) and CHROMOMETHYLASE 3 (CMT3), respectively; while asymmetric CHH methylation is either actively perpetuated by RdDM or maintained by a siRNA-independent process mediated by CMT2 (Cao and Jacobsen., 2003; Matzke and Mosher, 2014; Stroud et al., 2014). On the other hand, Arabidopsis encodes four active demethylases with 5-methylcytosine DNA glycosylase/lyase activities, namely DEMETER (DME), DME-Like 1 (DML1)/ROS1 (Repressor Of Silencing 1), DML2 and DML3 (Zhang et al., 2018). Both ROS1 and DME actively remove DNA methylation in all methylated cytosine contexts through a base excision repair (BER) mechanism (Gong et al., 2002; Mok et al., 2010). ROS1 is the active demethylase that has been the most characterized in vegetative tissues (Zhang et al., 2018). Mechanistically, ROS1 prunes siRNA-dependent or -independent DNA methylation at thousands of loci and this process often limits the spreading of DNA methylation at TE/repeat boundaries (Tang et al., 2016). Importantly, ROS1-directed removal of DNA methylation at specific promoters is critical to ensure a proper expression of genes required for developmental or abiotic stress responses (Yamamuro et al., 2014, Gong et al., 2002; Kim et al., 2019).

Several studies have unveiled a major role for DNA methylation in susceptibility against non-viral phytopathogens. For examples, DNA methylation-defective mutants of Arabidopsis are more resistant to the hemibiotrophic bacterium *Pto* DC3000 and the obligate biotrophic oomycete pathogen *Hyaloperonospora arabidopsidis* (Pavet et al., 2006, Yu et al., 2013; Dowen et al., 2012; Lopez Sanchez et al., 2016). Conversely, *ros1* mutants display enhanced susceptibility towards *Pto* DC3000 and *Hyaloperonospora arabidopsidis* (Yu et al., 2013; Lopez Sanchez et al., 2016), indicating that ROS1 promotes basal resistance against these pathogens. Furthermore, ROS1, DML2, DML3 and DME act cooperatively to orchestrate resistance towards *Fusarium oxysporum*, a devastating hemibiotrophic vascular fungal pathogen infecting a wide range of economically important crops (Le et al., 2014., Schumann et al., 2019). Altogether, these studies suggest that immune-responsive genes are likely to be regulated by DNA methylation and/or demethylation, which has been demonstrated at a subset of pathogen-responsive genes (Yu et al., 2013; Le et al., 2014; Lopez Sanchez et al., 2016; Schumann et al., 2019, Kong et al., 2020). These findings also suggest that demethylation of defence gene promoters

might ensure the DNA/chromatin binding of TFs during pathogen infection and/or elicitation, although this hypothesis has never been tested experimentally.

Here, we characterize Arabidopsis demethylase ROS1 in the context of antibacterial immunity. We first demonstrate that ROS1 positively regulates basal resistance against *Pto* DC3000 by antagonizing RdDM activity. Consistent with this observation, we found that the *TNL RESISTANCE METHYLATED GENE 1* (*RMG1*) contributes to basal resistance against *Pto* DC3000, and that ROS1-directed suppression of RdDM at *RMG1* promoter ensures a proper induction of this gene during PTI. Furthermore, we retrieved the whole set of flg22-responsive genes that are controlled by ROS1 and show that PAMP-triggered inducibility at two ROS1 targets, namely *RMG1* and *RLP43,* depends on the *cis*-effect of demethylation at their promoters. Furthermore, ROS1-directed demethylation at a specific sequence of the *RLP43* promoter, which carries a functional "W-box" WRKY-binding site, is critical for the DNA binding of PAMP-responsive WRKY TFs. Overall, this study reveals the extent to which ROS1 orchestrates Arabidopsis transcriptional immune reprogramming and unveils a crucial role for this demethylase in orchestrating WRKY-DNA binding at immune-responsive promoters.

Results

Arabidopsis *ROS1* promotes resistance towards *Pto* DC3000, mostly by antagonizing *DCL2* and/or *DCL3* functions

We have previously reported that *ros1* mutants exhibit enhanced spreading of *Pto* DC3000 in Arabidopsis leaf secondary veins (Yu *et al*., 2013). This phenotype was further confirmed here when *ros1-3* and *ros1-4* mutant leaves were wound-inoculated with a GFP-tagged *Pto* DC3000 (*Pto* DC3000-GFP) (Figure 1AB). In addition, an enhanced bacterial titer was observed in these *ros1* alleles dip-inoculated with *Pto* DC3000-GFP (Figure 1C). These data indicate that ROS1 positively regulates basal resistance against *Pto* DC3000. It has been shown that ROS1 antagonizes methylation at thousands of loci, which are methylated in a RdDM-dependent or -independent manner (Tang et al., 2016). To determine whether ROS1 could promote basal resistance by counteracting RdDM, we have performed the above assays in a *ros1-3 dcl2-1 dcl3-1* triple mutant (*ros1dcl23*), in which the biogenesis of 22 to

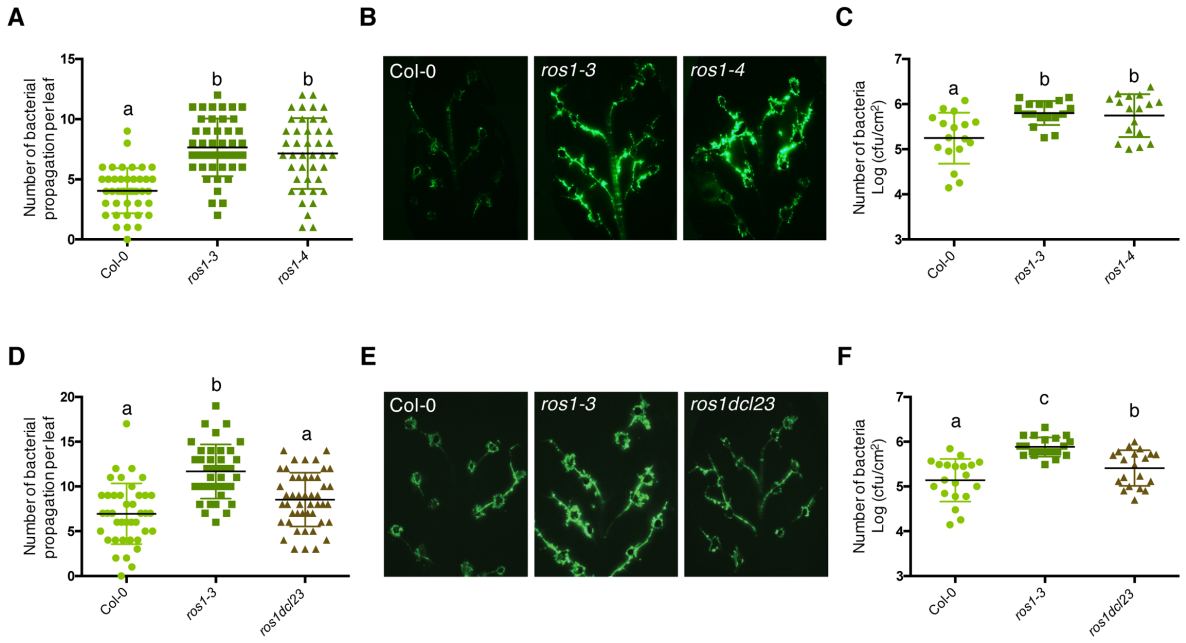

Figure 1. The enhanced *Pto* DC3000 disease susceptibility observed in *ros1*-infected mutants is mainly dependent on DCL2- and/or DCL3 functions.

A. Increased *Pto* DC3000 vascular propagation in the two independent *ros1* mutant alleles, *ros1-3* and *ros1-4*. Secondary veins of five-week-old Col-0, *ros1-3* and *ros1-4* mutants were inoculated with a virulent GFP-tagged *Pto* DC3000 strain (*Pto* DC3000-GFP) at 10^7 cfu ml^{-1} using the toothpick inoculation method. Inoculation was done on 6 secondary veins per leaf and 2 sites of inoculation per vein. The number of *Pto* DC3000-GFP spreading events from the wound inoculation sites was quantified after 3 days under UV light using a macrozoom. When the bacteria propagated away from any of the 12 inoculation sites, it was indexed as propagation with a possibility of maximum 18 propagations per leaf (see Material & Methods). The values from three independent experiments were considered for the comparative analysis. Statistical significance was assessed using a one-way ANOVA test and Tukey's multiple comparisons test.

B. Representative pictures of the GFP fluorescence observed at the whole leaf level on the plants presented in A.

C. Enhanced *Pto* DC3000 apoplastic growth in the two independent *ros1* mutant alleles, *ros1-3* and *ros1-4*. Five-week-old plants of Col-0, *ros1-3* and *ros1-4* mutants were dip-inoculated with *Pto* DC3000-GFP at 5 x 10^7 cfu ml^{-1}. Bacterial titers were monitored at 3 days post-inoculation (dpi). Three leaves out of four plants per line and from three independent experiments were considered for the comparative analysis. Statistical significance was assessed using a one-way ANOVA test and Tukey's multiple comparisons test.

D. Increased bacterial propagation in the vein observed in *ros1-3* is rescued in the *ros1dcl23* triple mutant. Secondary veins of five-week-old Col-0, *ros1-3* and the triple *ros1dcl23* mutants were inoculated as in A. and the results analysed as in A.

E. Representative pictures of the GFP fluorescence observed at the whole leaf level on the plants presented in D.

F. Enhanced *Pto* DC3000 apoplastic growth in *ros1* is partially rescued in the *ros1dcl23* background. Five-week-old plants of Col-0, *ros1-3* and *ros1dcl23* were inoculated as in C. and the results were analysed as in C.

153 24 nt siRNAs is abolished. Interestingly, we found that both the enhanced vascular propagation and
154 apoplastic growth of *Pto* DC3000-GFP detected in the *ros1-3* mutant were reduced in *ros1dcl23*
155 mutants, and almost comparable to the phenotypes of Col-0-infected plants (Figure 1D-F). These data
156 indicate that DCL2 and/or DCL3 are mainly responsible for the enhanced susceptible phenotypes
157 observed in *ros1-3*-infected mutants. They also suggest that some defence genes are likely
158 hypermethylated and silenced in the *ros1-3* mutants through the action of, at least in part, DCL2- and/or
159 DCL3-dependent siRNAs.
160
161 **The ROS1 target *RMG1* is a functional disease resistance gene that contributes to basal resistance**
162 **towards *Pto* DC3000**

163 ROS1 has previously been shown to ensure a proper flg22-triggered induction of *RMG1*, an orphan *TNL*
164 that is demethylated by ROS1 in its promoter (Yu et al., 2013). As a result, a strong reduction in flg22-
165 mediated inducibility of *RMG1* is observed in the absence of ROS1 (Figure 2D/F; Yu et al., 2013). To
166 investigate the possible contribution of *RMG1* in basal resistance against *Pto* DC3000, we have isolated
167 and characterized two independent T-DNA insertion lines, which lack *RMG1* mRNA in leaves treated
168 with flg22 compared to Col-0 (Figure 2A; Figure S1). Both mutants exhibited elevated bacterial vascular
169 propagation and apoplastic growth compared to Col-0-infected plants (Figure 2BC), indicating that
170 *RMG1* is a functional disease resistance gene that contributes to basal resistance towards *Pto* DC3000.
171 These data also suggest that the heightened susceptibility of the *ros1*-infected mutants might be in part
172 attributed to the silencing of *RMG1*.
173
174 **ROS1 limits the spreading of DNA methylation at the 3' boundary of a remnant RC/Helitron TE,**
175 **which is embedded in the *RMG1* promoter**

176 *RMG1* contains two remnant RC/Helitron TEs in its promoter: the distal repeat *AtREP4* (*At4TE29275)*
177 and the proximal repeat *AtREP11* (*At4TE29280*) (Figure 2D). *AtREP4* is targeted by 23-24 nt siRNAs
178 and methylated in the Arabidopsis reference accession Col-0, a regulatory process that presumably

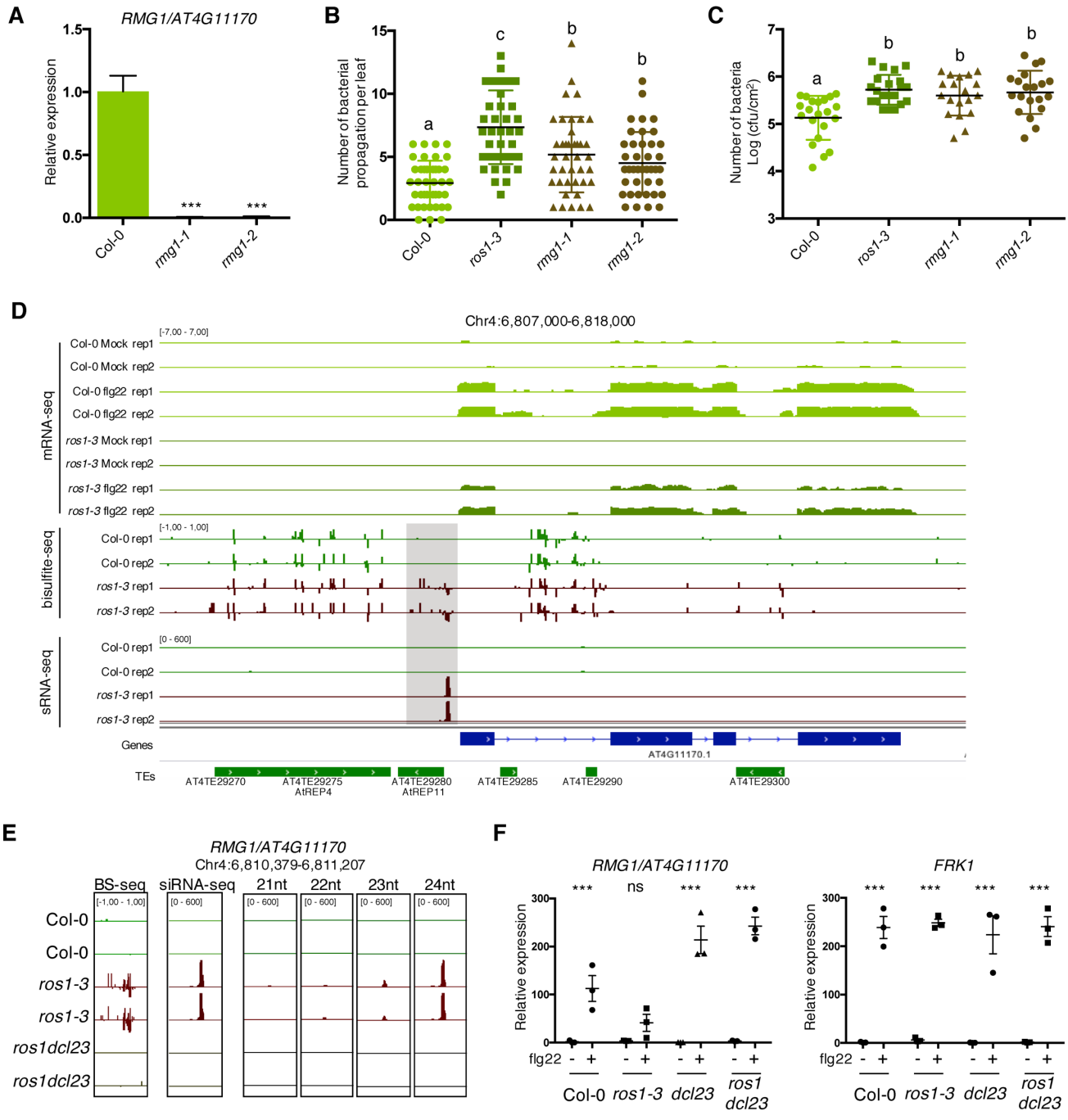

Figure 2. The *TNL* gene *RMG1* contributes to apoplastic and vascular resistance against *Pto* DC3000 and its flg22-triggered induction is negatively regulated by RdDM in the absence of ROS1.

A. *RMG1* mRNA levels in Col-0 and the two *rmg1* mutant alleles, namely *rmg1-1* and *rmg1-2,* were monitored by RT-qPCR at 6h after syringe-infiltration of mock (water) or 1 μM of flg22 peptide.

B. *RMG1* positively regulates vascular resistance towards *Pto* DC3000. Secondary veins of five-week-old Col-0, *ros1-3*, *rmg1-1* and *rmg1-2* plants were inoculated with *Pto* DC3000-GFP at 10^7 cfu ml^{-1} using the toothpick inoculation method. Inoculation was done on 6 secondary veins per leaf and 2 sites of inoculation per vein. The number of *Pto* DC3000-GFP spreading events from the wound inoculation sites was quantified after 3 days under UV light using a macrozoom. When the *Pto* DC3000-GFP propagated away from any of the 12 inoculation sites, it was indexed as propagation with a possibility of maximum 18 propagations per leaf. The values from three independent experiments were considered for the comparative analysis. Statistical significance was assessed using a one-way ANOVA test.

C. *RMG1* positively regulates apoplastic resistance towards *Pto* DC3000. Five-week-old Col-0, *ros1-3*, *rmg1-1* and *rmg1-2* plants were dip-inoculated with *Pto* DC3000-GFP at 5 x 10^7 cfu ml^{-1}. Bacterial titers were monitored at 3 days post-infection (dpi). Three leaves out of four plants per line and from three independent experiments were considered for the comparative analysis. Statistical significance was assessed using a one-way ANOVA test.

D. Flg22-triggered induction of *RMG1* is compromised in *ros1-3*-elicited mutant and correlates with an increased DNA methylation and siRNA levels at the remnant RC/Helitron TE *AtREP11*, and particularly at its 3' boundary. IGV snapshots showing mRNA levels (mRNA-seq) after syringe infiltration of mock (water) or 1 μM of flg22 peptide for Col-0 and *ros1-3*, and cytosine DNA methylation levels (Bs-Seq) and siRNA levels (sRNA-seq) in 5-week-old untreated rosette leaves of Col-0 and *ros1-3*, at the *RMG1* locus. The differentially methylated region (DMR) is highlighted by the dotted box.

E. Levels of different siRNA species at the 3' boundary of *AtREP11*. IGV snapshots representing the levels of methylation (BS-seq), total siRNA species (siRNA-seq) and different size of siRNA species (21nt, 22nt, 23nt and 24nt siRNAs) in 5-week-old rosette leaves of Col-0, *ros1-3* and *ros1dcl23*.

F. The flg22-triggered induction of *RMG1* is fully restored in *ros1dcl23*-elicited triple mutants. RT-qPCR analysis depicting *RMG1* and *FRK1* mRNA levels in Col-0, *ros1-3*, *dcl23* and *ros1dcl23* 5-week-old rosette leaves treated with either mock (water) or 1 μM of flg22 for 6h. The mRNA levels are relative to the level of *UBQ* transcripts. Statistical significance of flg22 treatment on expression was assessed using a two-way ANOVA test and a Sidak's multiple comparisons test.

maintain a low basal expression of this gene in untreated conditions (Yu et al., 2013). By contrast, *AtREP11* (*At4TE29280*), which is located 216 bp upstream of *RMG1* start codon, is unmethylated in Col-0 but hypermethylated in a *ros1* mutants, as previously demonstrated by a targeted bisulfite Sanger sequencing approach (Yu et al., 2013). These results were confirmed by using a whole-genome bisulfite sequencing (BS-seq) approach in rosette leaves of untreated Col-0 and *ros1-3* mutants (Figure 2D). We found that the hyper Differentially Methylated Region (hyperDMR) detected at the *AtREP11* repeat, was particularly pronounced at the 3' boundary of this remnant RC/Helitron TE in the *ros1-3* mutant, while this region was unmethylated in Col-0 plants (Figure 2D). This result is consistent with a role of ROS1 in limiting the spreading of DNA methylation at TE boundaries (Tang et al., 2016). To determine whether such hyperDMR could be directed by siRNAs, we monitored the accumulation of siRNAs at the *RMG1* promoter by analysing small RNA sequencing (sRNA-seq) datasets generated in rosette leaves of untreated Col-0, *ros1-3* and *ros1dcl23* mutants. While no siRNA was retrieved at the 3' boundary of *AtREP11* in Col-0 plants, we detected the accumulation of siRNA species of different sizes in the *ros1-3* mutant, ranging from low levels in the 21-22 nt species to high level in the 23-24 nt species (Figure 2DE). All these siRNA species were no longer produced in *ros1dcl23* mutants, a molecular effect which was associated with an absence of methylation at this ROS1-targeted region (Figure 2E). Collectively, these data indicate that DCL2 and/or DCL3-dependent siRNAs direct RdDM predominantly at the 3' boundary of *AtREP11* in the *ros1-3* mutant. They also suggest that, in Col-0 plants, ROS1 counteracts the biogenesis of DCL2- and DCL3-dependent siRNAs at this *RMG1* promoter region to restrict methylation spreading at the 3' boundary of *AtREP11*.

ROS1-directed suppression of siRNA biogenesis at the *RMG1* promoter is required for a proper induction of this gene during flg22 elicitation

We next assessed whether ROS1-directed suppression of RdDM at the *AtREP11* and its 3' boundary could be required for the proper induction of *RMG1* during flg22 elicitation. For this end, we challenged Col-0, *ros1-3*, *dcl2-1 dcl3-1* (*dcl23*) and *ros1dcl23* plants with either mock or flg22 for 6 hours and

205 further monitored the mRNA accumulation of *RMG1*. We found a compromised induction of *RMG1* in
206 the *ros1-3*-elicited mutant, which was not observed for *Flg22-induced Receptor-like Kinase 1* (*FRK1*),
207 which is not hypermethylated in *ros1-3* mutants and thus served as a control (Figure 2F; Figure S2;
208 Figure S3). By contrast, a full restoration of flg22-triggered inducibility of *RMG1* was observed in the
209 *ros1dcl23*-elicited mutant (Figure 2F; Figure S3). These data indicate that RdDM of *AtREP11* and its 3'
210 boundary, which is specifically detected in *ros1-3* mutants, negatively regulates the flg22 inducibility
211 of *RMG1*. They also suggest that ROS1-directed demethylation of this *RMG1* promoter region is crucial
212 to ensure a proper transcriptional activation of this gene during flg22 elicitation.

213

214 **ROS1 directs promoter demethylation of flg22-induced ROS1 targets, mostly by antagonizing**
215 ***DCL2* and/or *DCL3* functions**

216 To identify the whole set of immune-responsive genes that are regulated by ROS1, we further used an
217 RNA sequencing (RNA-seq) approach and applied a statistical analysis that retrieved differentially
218 accumulated transcripts in Col-0 *versus ros1-3* plants treated with either mock or flg22 for 6 hours.
219 Using this approach, we found 2076 differentially accumulated transcripts in flg22-challenged Col-0
220 plants, among which, 907 were less-induced and 1169 less-repressed in flg22-treated *ros1-3* mutants
221 (Figure 3A). To identify ROS1 putative primary targets, we next determined which of the 2943
222 hyperDMRs identified in untreated *ros1-3* plants were present in an interval covering the gene-body
223 plus 2Kb upstream and downstream of the 2076 flg22-sensitive *ROS1* targets. As a result of this analysis,
224 219 candidate genes were recovered, representing ~10% of the whole flg22-responsive and ROS1
225 regulated genes. Among them, 102 less-induced and 115 less-repressed genes were recovered (Figure
226 3A). To gain more insights into the regulatory function of ROS1 during PTI, we focused subsequent
227 analyses on flg22-induced ROS1 putative primary targets (Figure 3B; Figure S4). We found that the
228 overall increase of methylation levels at the 102 less-induced genes and at the whole 2943 ROS1 targets,
229 in *ros1-3* compared to Col-0 plants, was almost exclusively observed in 2 Kb upstream sequence regions
230 (Figure 3C). An increase in siRNA accumulation was also detected at both the promoters of the flg22-

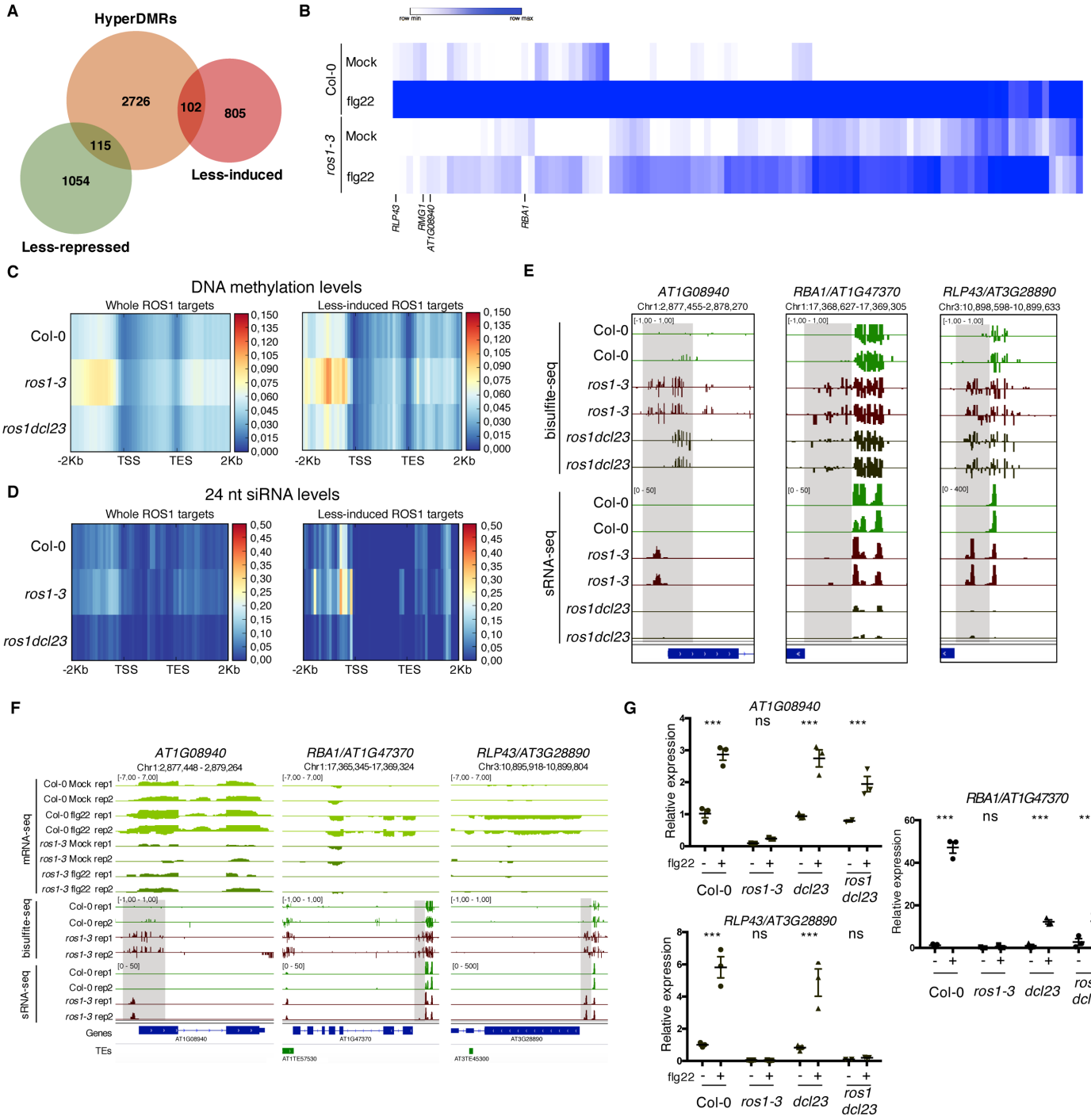

Figure 3. Genome-wide identification of flg22-responsive *ROS1* targets and characterisation of the role of RdDM in the methylation status of these genes in the absence of ROS1.

A. Proportion of flg22-responsive genes that are regulated by ROS1. One hundred and two flg22-responsive genes that are "less-induced" and 115 flg22-responsive genes that are "less-repressed" in *ros1-3*-elicited mutant exhibit hypermethylated DMRs (hyperDMRs). Venn diagram representing the overlap of genes presenting hyper-DMRs in the *ros1* mutant (in orange) with genes presenting a compromised induction (in red) or repression (in green) in *ros1-3* compared to Col-0 treated with mock (water) or 1 μM of flg22 for 6h.

B. Heat map representing the relative expression of the 102 less-induced genes in Col-0 and *ros1-3* treated with mock (water) or 1 μM of flg22 for 6h. Merged data from two independent biological replicates are presented.

C. Increased global DNA methylation levels observed in untreated *ros1-3* compared to Col-0 at the whole set of genes exhibiting hyperDMRs (left panel) and at the 102 less-induced genes (right panel) are restored in the *ros1dcl23* triple mutant. Heatmap representing global DNA methylation levels within regions comprising 2Kb upstream of the transcription start site (TSS), the gene body, and 2 Kb downstream of the transcription end site (TES) of the whole set of genes exhibiting hyperDMRs in *ros1-3 versus* Col-0 (left panel) and of the 102 less-induced genes (right panel). These heatmaps were generated from BS-seq datasets obtained from 5-week-old rosette leaves of Col-0, *ros1-3* and *ros1dcl23* mutants.

D. Increased 24 nt siRNA levels in *ros1-3* at the whole set of genes exhibiting hyperDMRs in *ros1-3 versus* Col-0 (left panel) and at the 102 less-induced genes (right panel) are restored in the *ros1dcl23* triple mutant. Heatmap representing 24-nt siRNA levels within regions comprising 2Kb upstream of the transcription start site (TSS), the gene body, and 2 Kb downstream of the transcription end site (TES) of the whole set of genes exhibiting hyperDMRs in *ros1-3 versus* Col-0 (left panel) and of the 102 less-induced genes (right panel). These heatmaps were generated from sRNA-seq datasets obtained from 5-week-old rosette leaves of untreated Col-0, *ros1-3* and *ros1dcl23* mutants. Average of the two replicates are represented.

E. Methylation levels at *RBA1* are partially restored in *ros1dcl23* whereas *RLP43* retains methylation levels similar to methylation levels observed in the single *ros1-3* mutant. IGV snapshots showing siRNA levels and methylation levels at the DMRs of *RBA1* and *RLP43* in Col-0, *ros1-3* and *ros1dcl23*.

F. IGV snapshots representing mRNA-seq data in Col-0 and *ros1-3* mutant in mock- and flg22-treated conditions as well as BS-seq and sRNA-seq of untreated Col-0 and *ros1-3* plants.

G. *RBA1* gene induction is partially restored whereas *RLP43* remains in a repressed state in *ros1dcl23*. RT-qPCR analyses from 5-week-old rosette leaves of Col-0, *ros1-3*, *dcl23* and *ros1dcl23* treated with either mock (water) or 1 μM of flg22 for 6h. The mRNA levels are relative to the level of *UBQ* transcripts. Statistical significance of flg22 treatment on expression was assessed using a two-way ANOVA test and a Sidak's multiple comparisons test.

induced and overall ROS1 targets in *ros1-3 versus* Col-0 plants (Figure 3D; Figure S5). By contrast, the overall enhanced DNA methylation and siRNA levels observed in *ros1-3* mutants at these loci was almost restored to Col-0 levels in *ros1dcl23* mutants (Figure 3C/D; Figure S5). The latter data suggest that ROS1 directs promoter demethylation mostly by antagonizing *DCL2* and/or *DCL3* functions.

ROS1 facilitates the flg22-triggered induction of three distinct targets by preventing hypermethylation at discrete regions in their promoters

We next selected, from our RNA-seq datasets, candidate genes that were strongly induced by flg22 in Col-0 plants and showing pronounced compromised flg22 inducibility in elicited *ros1-3* mutants (Figure 3B; Figure S4). These genes include the TIR-only resistance gene *RBA1* (*AT1G47370*), which was previously shown to be repressed by methylation in Col-0 and to recognize the bacterial effector HopBA1 in the *Arabidopsis thaliana* Ag-0 accession (Nishimura et al., 2017); the orphan *Receptor-Like Protein 43* (*RLP43*) (*AT3G28890*), which presents typical features of RLP PRRs (Steidele and Stam, 2020), and a phosphoglycerate mutase gene (*AT1G08940*) (Figure 3B). We further monitored their mRNA accumulation in Col-0, *ros1-3*, *dcl23* and *ros1dcl23* challenged with either mock or flg22 for 6 hours. The expression pattern of the phosphoglycerate mutase gene was similar to one of *RMG1*: the compromised flg22 induction of this gene was almost fully rescued in elicited *ros1dcl23* mutants, which is consistent with a loss of siRNA and DNA methylation at its hyperDMR in untreated *ros1dcl23* mutants (Figure 3E/G). The flg22-triggered induction of *RBA1* was restored in *ros1dcl23* to levels similar to *dcl23* mutants, but not to the same extent as in elicited Col-0 plants (Figure 3G). Furthermore, this effect was associated with a partial decrease in *RBA1* promoter methylation at the *RBA1* hyperDMR, in *ros1dcl23* compared to *ros1-3* mutants (Figure 3E). By contrast, *RLP43* remained fully silenced in the *ros1dcl23*-treated mutants, as in elicited *ros1-3* mutants, which is consistent with comparable levels of *RLP43* promoter methylation in both untreated mutants (Figure 3E). It is noteworthy that the unaltered *RLP43* hyperDMR detected in the *ros1dcl23* mutants, was associated with a moderate remaining accumulation of siRNAs, which was shifted from 23-24 nt siRNAs in *ros1-3* to 21 nt siRNAs in *ros1dcl23* mutants (Figure 3E; Figure S6). It was also accompanied by the presence of longer RNAs

(25 to 30 nt), which exhibit a preference for having an A at their 5'ends and that overlap with siRNAs produced from the hyperDMR, as observed for typical P4RNA species (Figure S6; Blevins et al., 2015; Zhai et al 2015; Yang et al., 2016). Because PolIV-dependent 21 nt siRNAs and P4RNAs are competent for RdDM (Yang et al., 2016; Panda et al., 2020), the above RNA entities might contribute to maintain RdDM at *RLP43* promoter in the *ros1dcl23* mutants, although RNA-independent mechanism(s) might additionally be involved. Collectively, these data indicate that the flg22-triggered induction of these three genes is facilitated by ROS1, which prevents hypermethylation at discrete regions in their promoters. They also indicate that their promoter hypermethylation detected in *ros1-3* mutants, can be fully or partially altered upon concomitant removal of DCL2 and DCL3, as found at the phosphoglycerate mutase and *RBA1* genes, respectively; or unchanged, as observed at the *RLP43* locus.

WRKY TFs bind to a single W-box element embedded in the middle of the demethylated promoter region of *RLP43*, thereby ensuring a proper flg22-triggered induction of this gene

Given that the ROS1-directed demethylation of a subset of defence gene promoters was required for their flg22-triggered induction (Figure 3), we hypothesized that these demethylated promoter sequences might contain functional binding sites for PAMP-responsive TFs. To test this possibility, we selected 26 flg22-induced ROS1 targets exhibiting discrete and dense hypermethylated regions in *ros1-3* mutants, along with a strong impaired induction in *ros1-3*-elicited mutants, and subjected their hyperDMR sequences to Genome Association Tester (GAT) (Figure S5A; Heger et al. 2013). This approach interrogates DNA Affinity Purification sequencing (DAP-seq) datasets of whole-genome Arabidopsis TF factor binding sites and assess whether any DAP-seq peak would overlap more with the input DNA sequence than expected by chance (O'Malley et al., 2016). By using this analysis, we found *in vitro* DNA binding of WRKY TFs at 14 out of 26 promoter-derived sequences tested (Figure 4A; Figure S7). Among these candidates, we retrieved *RMG1*, *RBA1* and *RLP43*, which exhibit *in vitro* DNA binding of several WRKYs in their promoter regions subjected to ROS1-directed demethylation (Figure 4A/B; Figures S7-9). Five out of these 14 candidate promoters also exhibit *in vivo* binding of the AtWRKY18 and AtWRKY40 based on chromatin immunoprecipitation sequencing (ChIP-seq) datasets

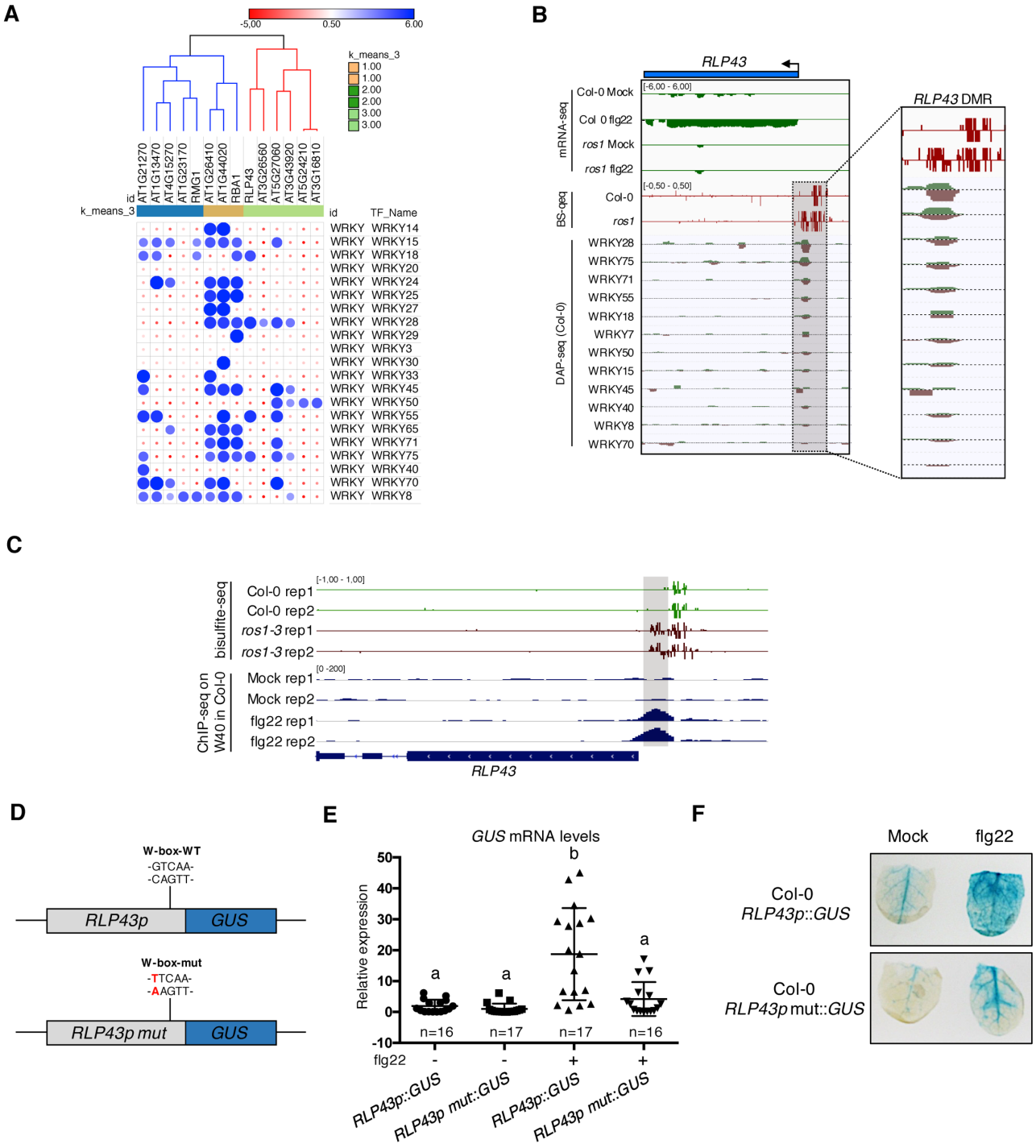

Figure 4. Several WRKY transcription factors bind to the demethylated region of the *RLP43* promoter, which contains a functional and flg22-responsive W-box *cis*-element.

A. A subgroup of the ROS1 targets exhibit an over-representation of WRKY DNA binding at the promoter regions corresponding the hyperDMRs that were retrieved in *ros1-3*. GAT analysis performed on publicly available DAP-sequencing data (O'Malley et al., 2016) identified WRKY transcription factors with significant enrichment in the regions corresponding to the hyperDMRs observed in *ros1-3* for the 14 stringent ROS1 primary targets.

B. Several WRKY transcription factors specifically bind at the region that is demethylated by ROS1 in the *RLP43* promoter. Snapshots representing, from top to bottom, mRNA-seq (Rep1), BS-seq (Rep1) and DAP-seq data at the *RLP43* locus. To better appreciate the overlap between the promoter region of *RLP43* subjected to ROS1-directed demethylation and the region where WRKY transcription factors bind to DNA, a zoom in is depicted at the level of the hyperDMR (box on the right panel).

C. A hemagglutinin (HA) epitope-tagged version of WRKY40 binds *in vivo* to the ROS1-targeted region of the *RLP43* promoter in a flg22-dependent manner. Snapshots depicting bisulfite sequencing data from 5-week-old rosette leaves of Col-0 and *ros1-3* mutant (Rep1) and ChIP-seq data performed on seedlings of *wrky40* mutants (SLAT collection of dSpm insertion line; Shen et al., 2007) complemented with WRKY40-HA treated with either mock (medium without flg22) or flg22 (medium supplemented with flg22) for 2h, at *RLP43* (Birkenbihl et al., 2017).

D. Scheme representing the *RLP43* transcriptional fusion constructs containing the WT W-box sequence (*RLP43p::GUS*) and the mutated W-box sequence (*RLP43p mut::GUS*).

E. The W-box *cis*-element at the *RLP43* promoter is functional and responsive to flg22. RT-qPCR analyses were performed to monitor the *GUS* mRNA levels in primary T1 transformants expressing either the *RLP43p::GUS* or *RLP43p mut::GUS* transgenes. For each individual, two leaves were syringe-infiltrated with mock (water) and two other leaves were treated the same way with flg22 at a concentration of 1 μM. The *GUS* mRNA levels are relative to the level of *UBQ* transcripts. Statistical significance was assessed using a one-way ANOVA test and a Tukey's multiple comparisons test.

F. The flg22-induced GUS activity is impaired in *RLP43p mut::GUS*-elicited plants. Representative pictures of GUS-stained leaves from 5-week-old rosette leaves of *RLP43p::GUS* or *RLP43pmut::GUS* primary transformants that were syringe-infiltrated with either mock or 1 μM of flg22 for 24h.

generated in flg22-challenged transgenic seedlings (Figure S10; Birkenbihl et al., 2017). Importantly, the chromatin association of these PAMP-responsive WRKYs was specifically detected during flg22 treatment, indicating that PTI signalling is required for this chromatin-based regulatory process (Figure S10). For example, the *in vivo* binding of AtWRKY40 at the *RLP43* promoter specifically occurs during flg22 elicitation and at the demethylated promoter region, which contains a W-box *cis*-regulatory element (Figure 4C; Birkenbihl et al., 2017). This observation prompted us to characterize this W-box in the context of PTI. For this end, we generated transcriptional reporters by fusing either the WT or the W-box point mutant upstream sequences of *RLP43* with the β-glucuronidase *GUS* reporter gene (Figure 4D). We found a strong reduction in GUS staining and mRNA levels in flg22-challenged leaves of primary transformants expressing the W-box mutant- *versus* the WT- versions of the *RLP43* transcriptional reporters (Figure 4E/F). These results imply that this W-box *cis*-element is functional and essential for the flg22-triggered transcriptional activation of *RLP43*. Nevertheless, the remaining GUS staining detected in the leaf vasculature of flg22-treated plants expressing the W-box mutant transgene suggests that other TFs must additionally contribute to the flg22-triggered transcriptional activation of *RLP43* in these tissues (Figure 4F). Collectively, these data indicate that the W-box *cis*-element located in the demethylated promoter region of the *RLP43* promoter is the site for WRKY TF binding. They also suggest that the flg22-triggered recruitment of WRKYs at the *RLP43* promoter is critical for the transcriptional activation of this gene during PTI.

ROS1-directed removal of DNA methylation at the *RLP43* promoter is necessary for DNA binding of AtWRKY18 and AtWRKY40

DNA methylation has previously been shown to inhibit, in some instances, TF-DNA binding (Watt and Molloy, 1988; Iguchi-Ariga and Schaffner, 1989; Tate and Bird, 1993; O'Malley et al., 2016). For example, a DNA Affinity Purification (DAP)-seq study performed with Col-0 genomic DNA revealed that ~75 % of Arabidopsis TFs are sensitive to DNA methylation (O'Malley et al., 2016). This was notably the case of several WRKY TFs used in their analysis (Figure 5A; O'Malley et al., 2016). This observation, along with the fact that the *ros1-3* mutation alters the flg22 induction of *RLP43* (Figures 3,4), suggests that the hypermethylation at its promoter observed in *ros1-3* mutants might interfere with

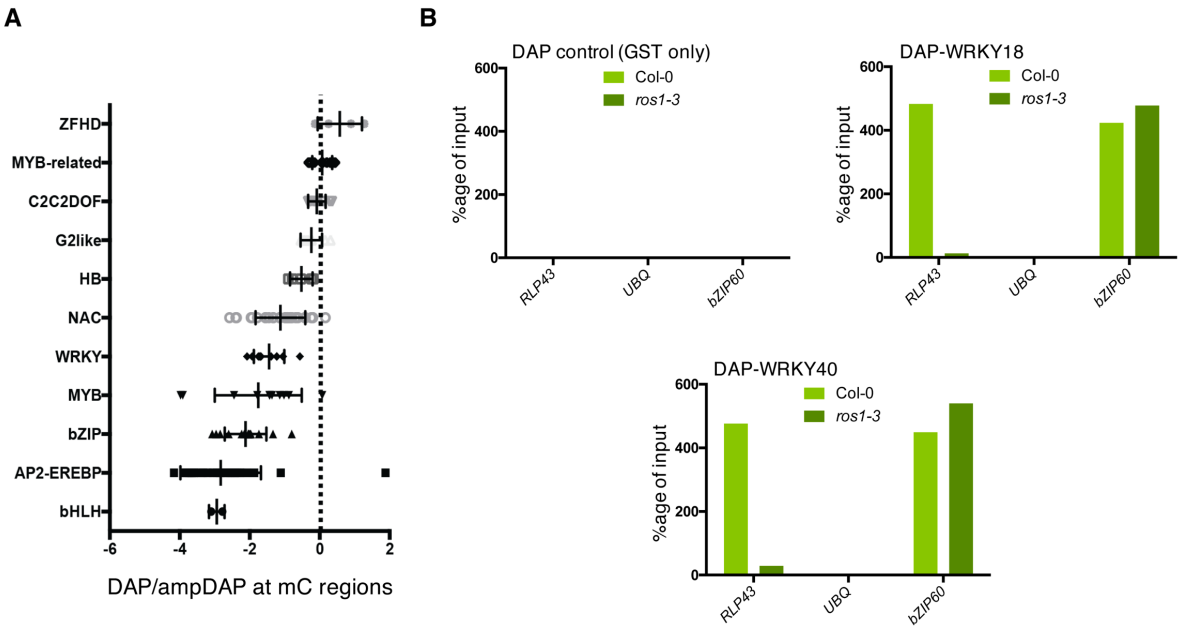

Figure 5. ROS1-directed demethylation is crucial for the DNA binding of WRKY18 and WRKY40 at the *RLP43* promoter.

A. DAP-seq data from O'Malley et al., 2016 showing that WRKY family members are generally sensitive to DNA methylation. Graph representing ratio of binding capacity in DAP vs. ampDAP data at regions methylated in Col-0 and for the different transcription factor family members used in this study.

B. The ability of WRKY18 and WRKY40 to bind DNA corresponding to the demethylated region of the *RLP43* promoter is abolished in the *ros1-3* mutant background. DAP-qPCR analysis at the *RLP43* promoter upon pull-down of Col-0 or *ros1-3* genomic DNA by GST (negative control), WRKY18-GST or WRKY40-GST. UBQ and *bZIP60* served as negative and positive controls, respectively.

WRKY TF-DNA binding. To test this hypothesis, we have used a DAP approach coupled with a quantitative PCR (DAP-qPCR) analysis. More specifically, we have expressed in bacteria Glutathion S-transferase (GST)-tagged AtWRKY18 and AtWRKY40, two well-characterized Arabidopsis WRKYs that are PAMP-responsive (Birkenbihl et al., 2017). Affinity-purified WRKYs were subsequently incubated with sheared genomic DNA from either Col-0 or *ros1-3* mutants and we further monitored WRKY DNA binding by qPCR analysis at the *RLP43* promoter. As a positive control for WRKY binding, we also amplified a promoter region of *bZIP60*, which is unmethylated in *ros1-3* mutants and bound by different PAMP-responsive WRKY TFs (Figures S2, S10; Birkenbihl et al. 2017). Using this DAP-qPCR approach, we found that both WRKY TFs exhibit strong and comparable enrichment at the *RLP43* and *bZIP60* promoters in the presence of Col-0 genomic DNA (Figure 5B; Figure S11), while no binding was found with GST alone (Figure 5B; Figure S11). By contrast, the DNA binding of these Arabidopsis WRKY TFs was almost fully abolished at the *RLP43* promoter with genomic DNA from *ros1-3* mutants, while it remained unaltered at the *bZIP60* promoter in the same conditions (Figure 5B; Figure S11). Collectively, these data provide evidence that the hypermethylation observed in *ros1-3* mutants at the *RLP43* promoter directly repels DNA binding of WRKY TFs.

ROS1-directed demethylation of *RMG1* and *RLP43* promoter-regulatory regions is causal for both flg22-triggered gene inducibility as well as basal resistance against *Pto* DC3000

The fact that the demethylation of a discrete *RLP43* promoter region, carrying a functional W-box *cis*-element, is required for WRKY TF DNA binding, suggests that the ROS1-directed suppression of promoter hypermethylation must be causal for flg22-triggered gene inducibility. To test this hypothesis, we generated Arabidopsis transgenic lines expressing a chimeric inverted repeat transgene bearing sequence identity to the *RMG1* and *RLP43* promoter regions that are subjected to ROS1-dependent demethylation (Figure 6A). By using this approach, we aimed to address whether artificial siRNAs in Col-0 would override the dominance of ROS1 over RdDM, thereby triggering hypermethylation at these promoter regions, which carry W-box *cis*-elements and DNA binding site of WRKY TFs (Figure 4; Figure S8). Molecular characterization by Northern blot and McrBC-qPCR analyses, respectively,

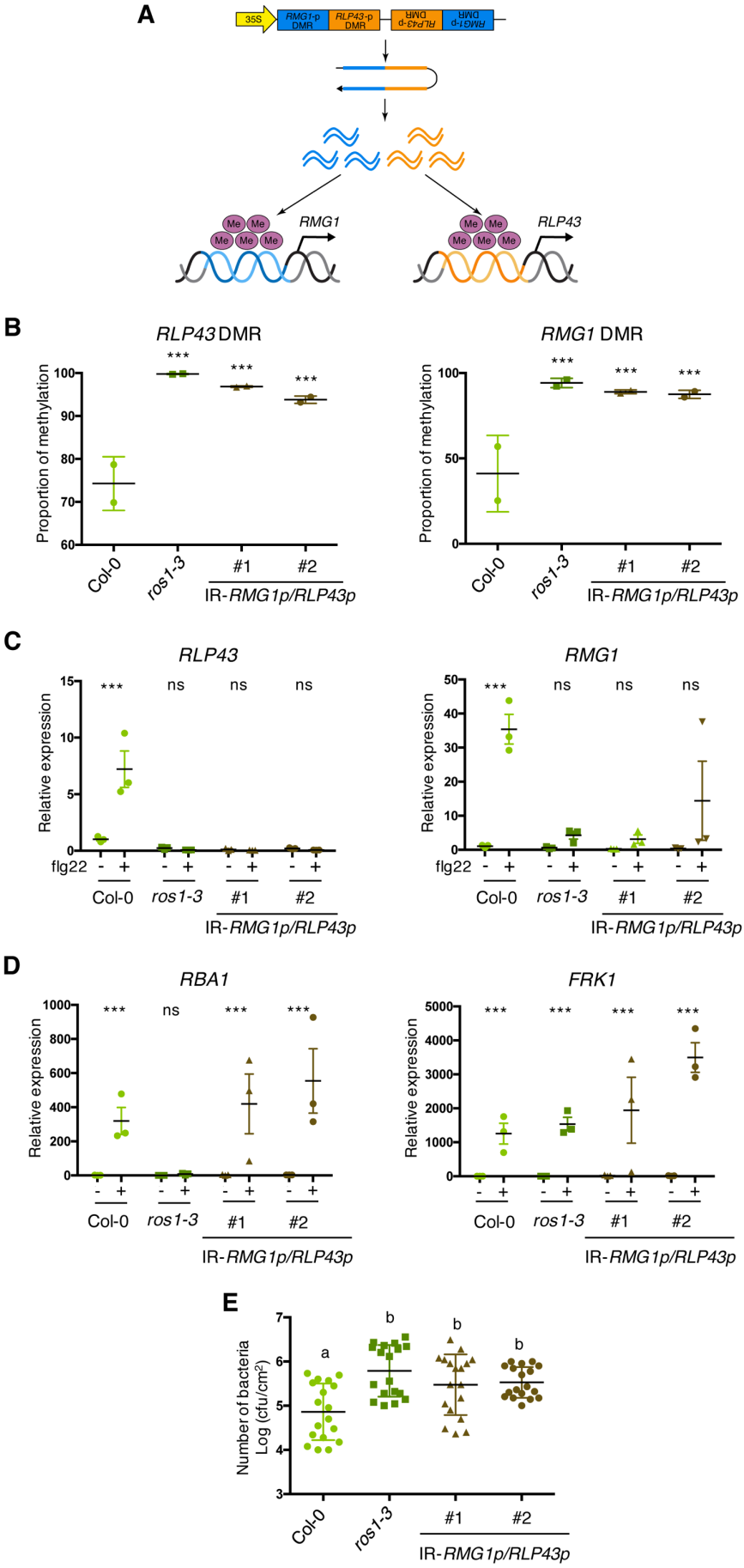

Figure 6. The artificial siRNA-directed targeting of remethylation at the *RMG1* and *RLP43* promoters impairs the flg22-triggered inducibility of these genes and enhances disease susceptibility towards *Pto* DC3000.

A. Scheme depicting the chimeric inverted repeat (IR) construct designed to simultaneously direct DNA remethylation at the *RMG1* and *RLP43* promoter regions. The IR-*RMG1p/RLP43p* contains sequences corresponding to the DNA sequence regions of *RMG1* (blue) and *RLP43* (orange) promoters that are demethylated by ROS1 in Col-0 and hypermethylated in *ros1* mutants. This inverted repeat transgene is driven by the constitutive 35S promoter, hence hypothesized to constitutively produce two populations of siRNA species designed to force remethylation of the *RMG1* and *RLP43* promoter regions that are normally demethylated by ROS1 in Col-0.

B. The *RMG1* and *RLP43* promoters exhibit hypermethylated in IR-*RMG1p/RLP43p* lines such as in *ros1-3* mutants. Genomic DNAs from Col-0, *ros1-3* and two independent IR-*RMG1p/RLP43p* lines (two biological replicates per line) were digested using McrBC and further analysed by qPCR. Ratio between digested DNA and undigested DNA was quantified to assess the proportion of methylation.

C. The flg22-triggered induction of *RMG1* and *RLP43* is impaired in the two independent IR-*RMG1p/RLP43p* lines. Five-week old rosette leaves of Col-0, *ros1-3* and two independent IR-*RMG1p/RLP43p* lines were syringe-infiltrated with either mock (water) or 1 μM of flg22 for 6h, and the mRNA levels of *RMG1* and *RLP43* were monitored by RT-qPCR analyses. The mRNA levels are relative to the level of *UBQ* transcripts. Statistical significance of flg22 treatment on expression was assessed using a two-way ANOVA test and a Sidak's multiple comparisons test.

D. The flg22-triggered induction of *RBA1* and *FRK1* is not affected in the two independent IR-*RMG1p/RLP43p* lines. Five-week old rosette leaves of Col-0, *ros1-3* and two independent IR-*RMG1p/RLP43p* lines were syringe-infiltrated with either mock (water) or 1 μM of flg22 for 6h, and the mRNA levels of *RBA1* and *FRK1* were monitored by RT-qPCR analyses. The mRNA levels are relative to the level of *UBQ* transcripts. Statistical significance of flg22 treatment on expression was assessed using a two-way ANOVA test and a Sidak's multiple comparisons test.

E. IR-*RMG1p/RLP43p* lines exhibit increased *Pto* DC3000 titer. Five-week-old plants of Col-0, *ros1-3* and two independent IR-*RMG1p/RLP43p* lines were dip-inoculated with *Pto* DC3000-GFP at 5 x 10^7 cfu ml^{-1}. Bacterial titers were monitored at 3 days post-infection (dpi). Three leaves out of four plants per line and from three independent experiments were considered for the comparative analysis. Statistical significance was assessed using a one-way ANOVA test and Tukey's multiple comparisons test.

revealed levels of siRNA accumulation and of methylation at these promoter regions that were comparable to the ones achieved in *ros1-3* mutants (Figures 6B; Figure S12), thereby validating our experimental strategy. We next challenged two independent IR-*RMG1p/RLP43p* transgenic lines with flg22 and monitored the levels of *RMG1* and *RLP43* mRNAs at 6 hours post-treatment. Significantly, we found that the induction of these genes was strongly altered in the two IR-*RMG1p/RLP43p* independent transgenic lines, almost to the same extent as in the *ros1*-elicited mutant background (Figure 6C; Figure S12C). By contrast, the flg22-triggered induction of *RBA1* and *FRK1* was comparable in Col-0 and IR-*RMG1p/RLP43p* transgenic lines (Figure 6D; Figure S12B), supporting a specific transcriptional silencing effect towards *RMG1* and *RLP43*. In addition, we found that IR-*RMG1p/RLP43p* lines displayed enhanced *Pto* DC3000 titers compared to Col-0-infected plants (Figure 6E), a phenotype resembling the one observed in *rmg1*-infected plants (Figure 2C). Collectively, these data demonstrate that the hypermethylation of these *RMG1* and *RLP43* discrete promoter regions is causal for the compromised flg22 induction of these genes and for increased susceptibility towards *Pto* DC3000. We conclude that ROS1-directed demethylation of these promoter regulatory sequences is critical for both flg22-triggered gene inducibility as well as antibacterial resistance.

Discussion

Active demethylation has emerged as a key regulatory mechanism of plant immunity. For examples, an enhanced susceptibility towards *Pto* DC3000 and *Hyaloperonospora arabidopsidis* was reported in *ros1* mutants (Yu et al., 2013; Lopez Sanchez et al., 2016). A heightened disease susceptibility towards *Fusarium oxysporum* was also found in the Arabidopsis *ros1 dml2 dml3* (*rdd*) mutant, and this phenotype was exacerbated by knocking-down *DME* in this background (Le et al., 2014, Schumann et al., 2019). Although these data indicate that demethylases promote basal resistance against unrelated phytopathogens, very little is known about the mechanisms involved in this process. Here, we showed that Arabidopsis *ros1* mutants exhibit enhanced growth and vascular propagation of *Pto* DC3000, two

366 phenotypes which were almost fully rescued in *ros1dcl23*-infected mutants (Figure 1). Therefore, ROS1
367 promotes basal resistance against *Pto* DC3000 mainly by antagonizing DCL2 and/or DCL3 functions.
368
369 We further found that the reprogramming of more than 2000 genes was altered in *ros1*-elicited mutants,
370 supporting a major role for ROS1 in controlling PAMP-triggered gene expression changes. Among these
371 genes, only ~ 10 % exhibit hyperDMRs in *ros1* mutants, and are thus potentially directly regulated by
372 ROS1. This is congruent with a previous transcriptome study conducted in *ros1* mutants infected with
373 *Hyaloperonospora arabidopsidis* (Lopez Sanchez et al., 2016), and suggests that the majority of biotic
374 stress-responsive genes are ROS1 secondary targets. This phenomenon is likely explained by the fact
375 that ROS1 directly controls the expression of a subset of central regulatory components of immune
376 responses, such as plant immune receptors, which have large impact on downstream signalling events.
377
378 In addition, we found that a similar proportion of ROS1 putative primary targets were up-regulated (102
379 genes) and down-regulated (115 genes) in response to flg22. This indicates that ROS1 is equally capable
380 of promoting the induction and repression of genes during flg22 elicitation. Some of these repressed
381 genes might act as plant defence repressors or, alternatively, as modulators of plant developmental or
382 physiological processes, possibly to redirect resources towards immunity and away from growth. It is
383 noteworthy that the role of active demethylation in promoting repression of genes has previously been
384 reported in the context of fruit ripening, whereby the tomato *ROS1* homolog *SlDML2* was found to
385 repress hundreds of ripening-related genes (Lang et al., 2017). Further studies are needed to determine
386 whether this feature of active demethylases could occur in the context of other biological processes.
387
388 We also performed a detailed analysis of the flg22-induced ROS1 putative primary targets. Most of
389 these genes exhibit hypermethylation at their promoters, an effect which was almost abolished in
390 *ros1dcl23* mutants (Figure 3CD). These data suggest that ROS1 antagonizes RdDM at these promoters,
391 presumably to facilitate their transcriptional activation during plant defence signalling. Consistent with
392 this hypothesis, we found that the impaired induction of *RMG1*, *RBA1* and of the phosphoglycerate
393 mutase genes observed in *ros1*-elicited plants was either fully or partially restored in *ros1dcl23*-elicited

394 mutants (Figures 2, 3). This was however not the case of *RLP43*, which remained fully silenced in
395 *ros1dcl23*-elicited mutants, a phenotype that was associated with a moderate gain of 21 nt siRNAs at
396 the *RLP43* hyperDMR in *ros1dcl23* mutants (Figure 3; Figure S6). This observation suggests that *DCL4*
397 and/or *DCL1* might, at least in part, compensate for the lack of *DCL2* and *DCL3* in the *ros1* mutants to
398 maintain RdDM at the *RLP43* promoter. This would be consistent with recent findings showing that
399 PolIV-dependent 21nt siRNA species, which are produced by DCL4, can trigger RdDM (Panda et al.,
400 2020). The longer RNAs detected at the *RLP43* hyperDMR in the *ros1dcl23* mutants (Figure 3; Figure
401 S6), and which exhibit classical features of P4RNAs (Figure S6; Blevins et al., 2015; Zhai et al 2015),
402 might also contribute to this phenomenon. The latter hypothesis is supported by the fact that P4RNA
403 species can efficiently direct DNA methylation at a large set of RdDM targets in the absence of DCL-
404 dependent siRNAs (Yang et al., 2016). Alternatively, and/or additionally, some yet-unknown RNA-
405 independent mechanism(s) might ensure the maintenance of DNA methylation at this locus in the
406 absence of ROS1, DCL2 and DCL3 factors.
407
408 Interestingly, our work demonstrates that the dominance of ROS1 over RdDM at two immune-
409 responsive gene promoters can be alleviated by artificially producing siRNAs against these genomic
410 regions (Figure 6). In particular, we showed that the stable expression of an inverted repeat transgene
411 bearing sequence homologies to the ROS1 targeted regions of *RMG1* and *RLP43* promoters, resulted in
412 their hypermethylation along with a compromised flg22-triggered induction of these genes (Figure 6).
413 Furthermore, we found that these transgenic lines exhibited an enhanced susceptibility towards *Pto*
414 DC3000, indicating that the silencing of these genes is sufficient to dampen basal resistance (Figure 6).
415 We are anticipating that this approach will be extensively used in the future to assess the regulatory
416 function of demethylases over any target(s) of interest. This strategy could also be exploited to transmit,
417 and possibly maintain, epialleles at specific demethylase target(s), and perhaps even when the transgene
418 is segregated away (if the intrinsic features of the targeted sequences are prone to form stable epialleles)
419 (Catoni et al., 2017, Li et al., 2020). Such an epi-editing strategy would be particularly relevant in crops
420 to prevent the unwanted expression of demethylase target(s) having negative effects on desirable trait(s).
421

Although the inactivation of demethylases is known to dampen resistance towards unrelated phytopathogens (Yu et al., 2013; Lopez Sanchez et al., 2016, Le et al., 2014, Schumann et al., 2019), the relevance of individual demethylase target in basal resistance remains ill-defined. Here, we have conducted an in-depth characterization of the ROS1 target *RMG1*. This orphan *TNL* gene contains two remnant RC/Helitron TEs in its promoter. The *AtREP4* distal repeat is highly methylated in all cytosine sequence contexts, a methylation pattern that is presumably required to maintain a low basal expression of this gene (possibly to prevent trade-off effects caused by its overexpression) (Yu et al., 2013, Deleris et al., 2016). The *AtREP11* proximal repeat is, conversely, unmethylated in Col-0 plants, and gain high level of methylation in *ros1* mutants, particularly at the 3' boundary of the *AtREP11* repeat, which contains W-box *cis*-elements and exhibits DNA binding of WRKY TFs (Figure 2; Figure S9; Yu et al., 2013). Significantly, both the accumulation of siRNAs and the hypermethylation observed in *ros1* mutant at this promoter region were abolished in the *ros1dcl23* mutant background (Figure 2). Furthermore, a full restoration of flg22-triggered inducibility of *RMG1* was observed in *ros1dcl23*-elicited mutants, indicating that siRNAs limit the induction of this gene in the *ros1*-elicited mutant background (Figure 2). Importantly, we found that mutations in *RMG1* enhanced disease susceptibility towards *Pto* DC3000, highlighting a major role of this *TNL* in basal resistance towards this bacterium (Figure 2). These data support previous findings showing that *NLRs* are not solely required for race-specific resistance but can also contribute to basal resistance, possibly by orchestrating PTI signalling and/or by mounting a weak ETI response through the recognition of virulence factors (Boccara et al., 2014; Canto-Pastor et al., 2019; Roth et al., 2017). Although *RMG1* is a functional ROS1 target, the concomitant silencing of several other defence genes in *ros1*, must additionally account for the increased disease susceptibility phenotypes observed in this mutant background.

DNA methylation has been shown to block DNA binding of some TFs *in vitro* (Watt and Molloy, 1988; Iguchi-Ariga and Schaffner, 1989; Tate and Bird, 1993; O'Malley et al., 2016). However, recent mechanistic studies at the promoter and/or enhancers of mammalian genes have highlighted a more complex picture, whereby TFs are either sensitive to DNA methylation or, alternatively, bind to methylated regions and in turn trigger their demethylation (Domcke et al., 2015; Schübeler, 2015; Yin

et al., 2017). In human cells, earlier studies suggested a role for active demethylation in modulating the chromatin accessibility of TFs in the context of bacterial elicitation or infection (Pacis et al., 2015). For example, a large set of genomic regions were found demethylated in human dendritic cells infected with *Mycobacterium tuberculosis*, leading to chromatin relaxation at enhancers carrying stress-responsive *cis*-elements (Pacis et al., 2015). Nevertheless, a recent study suggests that demethylation at these immune-responsive enhancers is unlikely required for the chromatin-based recruitment of TFs in these conditions, but is more probably occurring as a consequence of TFs binding at these genomic regions (Pacis et al., 2019). However, the exact role that demethylation could play in the DNA/chromatin accessibility for TFs remains ambiguous, because this work has not been conducted in human cells lacking individual demethylases. Here, we have exploited the genetically tractable model organism *Arabidopsis thaliana* to investigate this question at immune-responsive gene promoters. Interestingly, we found that the flg22-induced ROS1 primary targets exhibit an over-representation of *in vitro* WRKY TFs binding at discrete demethylated promoter regions (Figure 4; Figure S8). Some of these W-box elements are likely functional because *in vivo* recruitments of WRKYs was additionally observed at a subset of promoter regions in flg22-treated seedlings (Figure S11; Birkenbihl et al., 2017). By using a transcriptional fusion reporter approach, we also provided evidence that a single W-box element, centred in the *RLP43* promoter region that is demethylated by ROS1, was essential for flg22-triggered induction of this gene (Figure 4). Furthermore, we demonstrated that ROS1-directed demethylation of this *RLP43* promoter region facilitates DNA binding of the PAMP-responsive AtWRKY40 and AtWRKY18 (Figure 5; Figure S12; Birkenbihl et al., 2017). Based on these findings, we propose that ROS1 *cis*-regulates a subset of defence genes by ensuring binding of WRKY TFs at promoter regions, thereby allowing their rapid and pervasive transcription during PTI. Consistent with this *cis*-effect model, we observed a compromised flg22-triggered inducibility of *RLP43* and *RMG1* by forcing methylation at discrete promoter-regulatory regions, which are normally demethylated by ROS1, and that carry W-box elements (Figure 4, 6; Figure S9). ROS1-directed demethylation of defence gene promoters therefore likely provides a chromatin environment that is permissive for WRKY TFs binding, rendering these genes poised for transcriptional activation during plant defence signalling.

Plants and animals have evolved sophisticated epigenetic reprogramming prior and after fertilization. In

mammals, two waves of global demethylation and remethylation occur during germ cell development and embryogenesis, which tightly control transgenerational epigenetic inheritance (Heard and Martienssen, 2014). In plants, epigenetic reprogramming during sexual reproduction is less robust than in mammals, rendering epiallele transmission more possible through generations. This is supported by the description of multiple artificial and natural epialleles, recovered from various plant species (Weigel and Colot, 2012; Heard and Martienssen, 2014). In Arabidopsis, the dynamics and mechanisms of epigenetic reprogramming have been extensively characterized during the last decade. While high levels of CG methylation are observed in male meiocytes, microspores and sperm cells, a substantial erasure of CHH methylation occurs in the male germline (Calarco et al., 2012, Ibarra et al., 2012, Walker et al., 2018), which is regained during embryogenesis through RdDM (Bouyer et al., 2017, Kawakatsu et al., 2017). The latter phenomenon is accompanied by a restoration of active demethylation, which orchestrates removal of DNA methylation at incoming TEs/repeats and imprinted genes that display CG hypermethylation in the sperm cells, as a result of ROS1/DMLs repression in these cell types. Similarly, ROS1/DMLs might restore demethylation at defence gene promoters in the embryo, notably to ensure the reestablishment of poised W-box elements in the offspring (Deleris et al., 2016). Conversely, enhanced accumulation of endogenous siRNAs at these regulatory sequences is predicted to overcome demethylase reprogramming, as observed upon artificial production of siRNAs against *RMG1* and *RLP43* promoter regions carrying W-box *cis*-elements (Figures 3, 6; Figure S9), and would likewise favour epiallele formation. Investigating whether such hypothetical mechanism could occur in nature, and contributes to the emergence of immune-responsive expression variants, will be essential to unravel the mechanisms by which environmental constraints drive the selection of new phenotypes during plant evolution and adaptation.

Material and Method

Plant material and growth conditions

Arabidopsis plants were grown at 22°C in short day conditions (8h light, 16h dark) and all experiments were performed on 5-week-old rosette leaves.

Mutant lines

Besides WT Col-0, the single mutants *ros1-3*, *ros1-4* (Penterman et al., 2007), *rmg1-1* (SALK_007034) and *rmg1-2* (SALK_023944), the double *dcl2-1 dcl3-1* (*dcl23*) (Xie et al., 2004), and the triple *ros1-3 dcl2-1 dcl3-1* (*ros1dcl23*) mutants were used in this study.

Plasmids and constructs

The WRKY-GST constructs

The pGEX-2TM-WRKY18 and pGEX-2TM -WRKY40 allow bacterial expression of the N-ter GST-tagged version of full-length WRKY18 and WRKY40 (gift from Prof. Imre Somssich, MPI Cologne). Full-length cDNAs of each WRKYs were amplified and cloned into Gateway compatible entry vectors and subsequently recombined into the pGEX-2TM-GW destination vector.

The IR-*RMG1p/RLP43p inverted repeat construct*

The IR-*RMG1p/RLP43p* construct is a chimeric inverted repeat construct composed in each arm of the 180 bp and 137 bp sequences that are demethylated by ROS1 at the *RMG1* and *RLP43* promoters, respectively (with the intron of the petunia chalcone synthase gene *CHSA* in between). The IR-*RMG1p/RLP43p* was synthesized and inserted by restriction enzymatic digestion into the modified pDON221-P5-P2 vector by GenScript®. A double recombination of this vector together with the pDON221-P1-P5r plasmid carrying the Cauliflower Mosaic Virus (CaMV) 35S promoter sequence in the pB7WG Gateway destination vector was performed to obtain the destination plasmid containing the 35Sp::IR-*RMG1p/RLP43p* construct. The plasmid was further introduced into the *Agrobacterium tumefaciens* C58C1 strain, which was then used for *Agrobacterium*-mediated plant transformation (Clough and Bent, 1998).

RLP43p::GUS and RLP43pmut::GUS

The 1.5 Kb sequence located upstream of the start codon of *RLP43* was cloned in the pENTR/D-TOPO vector and recombined in the pBGWFS7 binary destination vector, containing the *GUS* reporter gene. Site-directed mutagenesis was performed with primers GAACGCCTCGTAGGTTCAAGCTGTGTTGGAAT and ATTCCAACACAGCTTGAACCTACGAGGCGTTC to mutate the W-box from GGTCAA to GTTCAA. Both *RLP43p::GUS* and *RLP43pmut::GUS* constructs were transformed in the Col-0 accession by

Agrobacterium-mediated method (Clough & Bent, 1998). Primary transformants were selected with Basta herbicide (10 µg/mL). GUS staining as well as RT-qPCR analysis on *GUS* transcripts were performed on at least 16 individual primary transformants for WT and mutated constructs. The primary transformants were infiltrated with either mock (water) or 1 µM of flg22 for 24 hours and RT-qPCR further performed.

Bacterial secondary leaf vein inoculation and quantification of the bacterial spreading phenotypes

Bacterial propagation in the secondary veins was assessed as described previously (Yu et al., 2013). About 16 leaves from four plants per condition were inoculated with a toothpick that was previously dipped in an inoculum of GFP-tagged *Pto* DC3000 at a concentration of 5 x 10^6 cfu/ml (OD_{600} of 0.2 corresponds to 10 ^{8}cfu/ml). Inoculation was done on 6 secondary veins per leaf and 2 sites of inoculation per vein. The number of bacterial spreading events from the wound inoculation sites was quantified after 3 days under UV light using a macrozoom (Olympus MVX10). When the bacteria propagated away from any of the 12 inoculation sites, it was indexed as propagation with a possibility of maximum 18 propagations per leaf. The values from three independent experiments were considered for the comparative analysis. Statistical significance was assessed using a one-way ANOVA test and Tukey's multiple comparisons test.

Bacteria growth assays

Four plants per condition were dip-inoculated using *Pto* DC3000 at 5 x 10^7 cfu/ml supplemented with 0.02 % Silwet L-77, and immediately placed in chambers with high humidity. Bacterial growth was determined 3 days post-infection. For the quantification, infected leaves were harvested, washed for one minute in 70 % (v/v) EtOH and one minute in water. Leaf discs with a diameter of 4 mm have been excised, grinded and homogenized in 100 µl of water. Each data point consists of four-leaf discs. Ten µl of each homogenate were then plated undiluted and at different dilutions. Bacterial growth was determined after 36 h of incubation at 28°C by colony counting.

Quantitative RT-PCR (RT-qPCR) analyses

Total Arabidopsis RNAs were extracted using Nucleospin RNA plant kit (Macherey Nagel). Five hundred ng of DNase-treated RNA were reverse transcribed using qScript cDNA Supermix (Quanta Biosciences®). cDNA was then amplified by real time PCR reactions using Takyon SYBR Green Supermix (Eurogentec®) and gene specific primers. Expression was normalized to that of the Arabidopsis housekeeping gene Ubiquitin. Sequences of the primers are listed in Supplementary Table 1.

McrBC digestion followed by qPCR

McrBC digestion was performed as described previously (Bond et al., 2015) on 200 ng of DNA. The reaction buffer was composed of 1X NEB Buffer 2, 20 µg BSA, 1 mM GTP in a final volume of 100 µL. Then, sample was split in two tubes. One hundred ng of DNA was digested at 37 °C overnight with 10 U of McrBC (New England Biolabs) in one tube, while the enzyme was not added in the control tube. The reactions were inactivated at 65 °C during 20 min. Six ng of DNA was then amplified by real time PCR reactions using Takyon SYBR Green Supermix (Eurogentec®) and gene-specific primers.

DNA Affinity Purification (DAP) followed by qPCR analysis

DNA affinity purification (DAP) followed by qPCR was performed following a protocol modified from Bartlett et al. 2017.

DNA preparation

Genomic DNA was extracted using the CTAB (Hexadecyl trimethyl-ammonium bromide) protocol (Doyle and Doyle, 1990). Then, five µg genomic DNA were sonicated to obtain DNA fragments of around 200-300 bp long. Sonicated DNA was then precipitated and resuspended in EB buffer (10mM Tris-CL, pH=8,5).

Protein expression

For each transcription factor or control expressing GST alone, 200 mL culture of *E. coli* Rosetta strain, carrying pGEX-TW-WRKY or empty vector for the GST alone, at a DO_{600nm}=0,3-0,6 were induced with 1 mM IPTG during 1 hour at 37°C. Expression of the WRKYs was then confirmed on a Coomassie gel.

DNA-affinity purification

Bacteria pellet were lysed and sonicated for 10 cycles of 10 seconds. The supernatants containing expressed proteins were incubated with washed MagneGST beads (Promega) (25 µL per transcription factor and per DNA sample tested) during 1h at room temperature with gentle rotation. After five steps of washing with 1X PBS + NP40 (0,005%) and three steps with 1X PBS, beads bound with GST-WRKYs were mixed with 200 ng of sonicated DNAs and incubated 1h at room temperature with gentle rotation. Samples were then washed five times with 1X PBS + NP40 (0,005%) and two times with 1X PBS. Beads were then resuspended in 25 µL EB (10mM Tris-CL, pH=8,5) and the samples heated during 10 minutes at 98°C. Supernatant was further kept for qPCR analysis.

qPCR following DAP

The equivalent of 1 µL of immunoprecipitated DNA was then amplified by real time PCR reactions using Takyon SYBR Green Supermix (Eurogentec®) and gene specific primers.

Northern blot

Accumulation of low molecular weight RNAs was assessed by Low Molecular Weight Northern blot analysis as previously described (Navarro et al., 2008). Total RNA was extracted using TRIzol reagent and stabilized in 50% formamide and 30 µg of total RNAs were used. To generate specific 32P-radiolabelled probes, regions of 150 bp to 300 bp were amplified from the plasmids using gene specific primers listed in Supplementary Table 1 and the amplicons were labelled by random priming (Prime-a-Gene® Labeling System, Promega). U6 was used as an equal loading control.

GUS staining assay

GUS staining was performed as described previously (Zervudacki et al., 2018). The staining was performed on at least 16 individual T1 plants. Two leaves per plant were infiltrated either with mock (water) or with 1 µM flg22.

Whole genome bisulfite, mRNA and small RNA sequencing and bioinformatic datamining

Small RNA reads processing

Total RNAs from 5-week-old leaves of Col-0, *ros1-3* and *ros1dcl23* mutants were used for small RNA deep-sequencing (two independent biological replicates were used for this analysis). Custom libraries for ~16-30 nt RNAs were constructed and sequenced by Fasteris®. We filtered all six libraries based on base-call quality of Q20 (99% base call accuracy). We then selected a subset of read size comprised between 16 and 30 nt for further analyses. Reads were mapped to TAIR10 genome using bowtie (Langmead et al., 2009), allowing zero mismatches, and further normalized using a Reads Per Kilobase Million (RPKM) approach. A strong uphill correlation was observed between replicates: 0.79 between Col-0 replicates, 0.81 between *ros1-3* replicates and 0.77 between *ros1dcl23* replicates.

Identification of flg22 differentially expressed genes

Total RNAs from 5-week-old leaves of Col-0 and *ros1-3* mutants were syringe-infiltrated with either mock (water) or 1 µM of flg22 for 6 hours and mRNA-seq experiments further carried-out (two independent biological replicates were used for this analysis). Reads were mapped to the TAIR10 genome using TopHat (v2.0.8b) (Kim et al., 2013) and allowing 2 mismatches. In this analysis, reads reporting multiple alignments were tolerated. The score was divided by the total number of hits. Using the stranded mRNA protocol, read counts were reported separately for sense and antisense transcripts. Uninformative annotations were filtered out by keeping only annotations showing at least one count per million (CPM) in 2 samples simultaneously. After count per million computations, if a gene had only one read reported in only one sample, it was discarded. But if it had one read mapped in at least 2 samples, it was kept. This step is performed to eliminate non expressed and non-informative genes that tend to produce noise and ultimately bias internal variance estimations, needed for further steps. Trimmed mean of M-values (TMM) normalization was performed followed by a likelihood ratio test.

The resulting p-values were adjusted using Benjamini and Hochberg's approach (Benjamini and Hochberg, 1995). An annotation was considered differentially expressed when a log2 fold-change> 0 and a p-value <0.05 was observed in 'flg22' vs 'mock' comparison.

Identification of flg22 differentially expressed genes that are regulated by ROS1.

We identified differentially expressed genes separately for Col-0 and *ros1-3* samples in elicited *vs* mock conditions. For each gene, we kept the information of the type of regulation: 'induced' when the p-value after correction is <=0.05 and the log2 fold-change >0, 'repressed', when the p-value after correction is <=0.05 and the log2 fold-change <0 or 'none' for the rest of the genes.

In the following analysis, we considered four cases. If there is an induction in Col-0 and there is no regulation in *ros1-3* or the regulation in *ros1-3* is at least two times less important than that of Col-0 (based on fold-change), the gene will be considered as 'less-induced'. Likewise, a 'repressed' gene in Col-0 will be considered as 'less-repressed' if its repression is at least two times less important or if there is no regulation in *ros1-3*.

Bisulfite-sequencing (Bs-Seq) data mining

Genomic DNAs from 5-week-old leaves of Col-0, *ros1-3* and *ros1dcl23* were extracted using DNeasy plant mini kit (Qiagen) and used for bisulfite sequencing (Bs-Seq) analyses (two independent biological replicates were used for this analysis). We filtered-out low quality reads using trim galore and aligned to TAIR10 genome using Bismark (Krueger et al., 2011). Mapping steps were followed by a cytosine methylation call.

Identification of differentially methylated regions (DMRs)

The methodology was conducted as previously reported (Qian et al., 2012) and performed for each biological replicate separately. For Differentially Methylated Cytosines call (DMCs), we kept cytosines having a read coverage of at least 2 and less than 100 in both the wild-type and mutant samples. A cytosine was considered differentially methylated when the p-value from the two-tailed fisher's test was < 0.05, hypermethylated if the level of methylation in the mutant was greater than the WT and hypomethylated in the opposite case. Differentially Methylated Regions (DMRs) were retrieved using a sliding windows strategy. We divided the genome into 1000 bp regions with a sliding window of 500 bp. We kept the regions which contained at least 5 DMCs and we redefined the coordinate as the first and last DMCs of that region. When the distance between two regions was less than 100bp with at least 10 DMCs, they were concatenated into one window. Regions with ambiguous hypermethylated and hypomethylated DMCs were discarded. Finally, we only kept regions that overlap in both replicates with at least 10 DMCs and a 10% methylation level shift in one of the 3 cytosine contexts when comparing Col-0 to *ros1-3*.

Cross-referencing mRNA-Seq and Bisulfite-Seq data

For this analysis, we focused on protein-coding genes having a hyper-DMR "within 2Kb" (*i.e.* the region covering the gene-body plus 2Kb upstream and downstream). Using this method, we selected 2944 protein coding genes. This list was then crossed with the list of "less-induced genes", which allowed us to retrieve 102 candidates for further analyses.

Meta-analyses of "less-induced genes" having a hyper-DMR "within 2Kb"

We used deeptools (Ramírez et al*.,* 2016) with sliding genomic windows of 100bp to visualize average methylation levels of 102 candidates in Col-0, *ros1-3* and *ros1dcl23* samples. The rest of 2944 genes having a hyper-DMR within 2kb were used as control. With the same approach we compared families of small RNAs in all three backgrounds. An analysis was performed for 21-22nt and 23-24nt families separately after a read-per-million normalization.

GAT analysis conducted on promoter sequence regions from stringent flg22-induced ROS1 targets

To assess whether Arabidopsis transcription factors (TFs) could bind to the DNA promoter regions from flg22-induced ROS1 targets, we first selected a subset of 30 stringent ROS1 targets (exhibiting dense hyperDMR in their promoter regions and which are strongly impaired in their induction in the *ros1*-elicited mutant background). We used the Genomic Association Tester (GAT) (Heger et al*.,* 2013) to find significant association between DMR regions and experimentally validated transcription factor binding sites from previously published DAP-seq data (O'Malley *et. al,* 2016). A transcription factor was kept when its *p*-value and fold-change of association were respectively <0.05 and >1. K means analysis was performed to see what genes group together when we take the WRKY binding profile as criterion. The distance tree displayed on top of the heatmap was obtained using the GAT scores to perform a hierarchical clustering, here we computed a one minus Pearson correlation to draw distances. The size of the circle represents the log2-fold-change of GAT analysis (a higher log2-fold-change, corresponding to a bigger circle, means the TF binds more often on this particular promoter than in 1000 simulations of randomly assigned genomic intervals of the same size).

Acknowledgements

We thank Imre Somssich for providing the pGEX-TM-WRKY40 plasmid and the ChIP-seq raw datasets ahead of publication; Robert Fischer for providing the *ros1-3* and *ros1-4* alleles; Florence Jay for its contribution to the selection of the *ros1-3 dcl2-1 dcl3-1* mutants, and all the members of the Navarro lab for their inputs, discussions and critical reading of the manuscript. This work was supported by a European Research Council (ERC) Starting Grant "Silencing and Immunity" (281749), and an Agence Nationale pour la Recherche (ANR) "NEPHRON" (ANR-18-CE20-0020), both granted to LN. TH received additional support by a Marie Curie Individual Fellowship (EU project 661715 – BASILA) and a post-doc funding from the "Fondation Pierre-Gilles de Genes". JW and MSR received support from the programme "Investissements d'avenir" implemented by ANR (ANR-10-LABX-54 MEMO LIFE, ANR-10-IDEX-0001-02PSL).

References

Bartlett, A., O'Malley, R.C., Huang, S.-S.C., Galli, M., Nery, J.R., Gallavotti, A., Ecker, J.R., 2017. Mapping genome-wide transcription-factor binding sites using DAP-seq. Nat Protoc 12, 1659–1672.

Bernoux, M., Ve, T., Williams, S., Warren, C., Hatters, D., Valkov, E., Zhang, X., Ellis, J.G., Kobe, B., Dodds, P.N., 2011. Structural and functional analysis of a plant resistance protein TIR domain reveals interfaces for self-association, signaling, and autoregulation. Cell Host Microbe 9, 200–211.

Benjamini, Y., Hochberg, Y., 1995. Controlling the False Discovery Rate: A Practical and Powerful Approach to Multiple Testing. Journal of the Royal Statistical Society. Series B (Methodological) 57, 289–300.

Birkenbihl, R.P., Kracher, B., Roccaro, M., Somssich, I.E., 2017. Induced Genome-Wide Binding of Three Arabidopsis WRKY Transcription Factors during Early MAMP-Triggered Immunity. Plant Cell 29, 20–38.

Blevins, T., Podicheti, R., Mishra, V., Marasco, M., Wang, J., Rusch, D., Tang, H., Pikaard, C.S., 2015. Identification of Pol IV and RDR2-dependent precursors of 24 nt siRNAs guiding de novo DNA methylation in Arabidopsis. Elife 4, e09591.

Boccara, M., Sarazin, A., Thiébeauld, O., Jay, F., Voinnet, O., Navarro, L., Colot, V., 2014. The Arabidopsis miR472-RDR6 silencing pathway modulates PAMP- and effector-triggered immunity through the post-transcriptional control of disease resistance genes. PLoS Pathog. 10, e1003883.

Boller, T., Felix, G., 2009. A renaissance of elicitors: perception of microbe-associated molecular patterns and danger signals by pattern-recognition receptors. Annu Rev Plant Biol 60, 379–406.

Bond, D.M., Baulcombe, D.C., 2015. Epigenetic transitions leading to heritable, RNA-mediated de novo silencing in *Arabidopsis thaliana*. Proc. Natl. Acad. Sci. U.S.A. 112, 917–922.

Boutrot, F., Zipfel, C., 2017. Function, Discovery, and Exploitation of Plant Pattern Recognition Receptors for Broad-Spectrum Disease Resistance. Annu Rev Phytopathol 55, 257–286.

Bouyer, D., Kramdi, A., Kassam, M., Heese, M., Schnittger, A., Roudier, F., Colot, V., 2017. DNA methylation dynamics during early plant life. Genome Biol. 18, 179.

Calarco, J.P., Borges, F., Donoghue, M.T.A., Van Ex, F., Jullien, P.E., Lopes, T., Gardner, R., Berger, F., Feijó, J.A., Becker, J.D., Martienssen, R.A., 2012. Reprogramming of DNA methylation in pollen guides epigenetic inheritance via small RNA. Cell 151, 194–205.

Canto-Pastor, A., Santos, B.A.M.C., Valli, A.A., Summers, W., Schornack, S., Baulcombe, D.C., 2019. Enhanced resistance to bacterial and oomycete pathogens by short tandem target mimic RNAs in tomato. Proc. Natl. Acad. Sci. U.S.A. 116, 2755–2760.

Cao, X., Jacobsen, S.E., 2002. Role of the Arabidopsis DRM methyltransferases in *de novo* DNA methylation and gene silencing. Curr. Biol. 12, 1138–1144.

Cao, X., Aufsatz, W., Zilberman, D., Mette, M.F., Huang, M.S., Matzke, M., Jacobsen, S.E., 2003. Role of the DRM and CMT3 methyltransferases in RNA-directed DNA methylation. Curr. Biol. 13, 2212–2217.

Catoni, M., Griffiths, J., Becker, C., Zabet, N.R., Bayon, C., Dapp, M., Lieberman-Lazarovich, M., Weigel, D., Paszkowski, J., 2017. DNA sequence properties that predict susceptibility to epiallelic switching. EMBO J. 36, 617–628.

Chan, S.W.-L., Zilberman, D., Xie, Z., Johansen, L.K., Carrington, J.C., Jacobsen, S.E., 2004. RNA silencing genes control de novo DNA methylation. Science 303, 1336.

Clough, S.J., Bent, A.F., 1998. Floral dip: a simplified method for Agrobacterium-mediated transformation of *Arabidopsis thaliana*. Plant J. 16, 735–743.

Couto, D., Zipfel, C., 2016. Regulation of pattern recognition receptor signalling in plants. Nat. Rev. Immunol. 16, 537–552.

Deleris, A., Halter, T., Navarro, L., 2016. DNA Methylation and Demethylation in Plant Immunity. Annu Rev Phytopathol 54, 579–603.

Domcke, S., Bardet, A.F., Adrian Ginno, P., Hartl, D., Burger, L., Schübeler, D., 2015. Competition between DNA methylation and transcription factors determines binding of NRF1. Nature 528, 575–579.

Dowen, R.H., Pelizzola, M., Schmitz, R.J., Lister, R., Dowen, J.M., Nery, J.R., Dixon, J.E., Ecker, J.R., 2012. Widespread dynamic DNA methylation in response to biotic stress. Proc. Natl. Acad. Sci. U.S.A. 109, E2183-2191.

Doyle, J.J. and Doyle, J. L., 1990. Isolation of plant DNA from fresh tissue. Focus 12, 13-15

Gong, Z., Morales-Ruiz, T., Ariza, R.R., Roldán-Arjona, T., David, L., Zhu, J.K., 2002. ROS1, a repressor of transcriptional gene silencing in Arabidopsis, encodes a DNA glycosylase/lyase. Cell 111, 803–814.

Halter, T., Navarro, L., 2015. Multilayer and interconnected post-transcriptional and co-transcriptional control of plant NLRs. Curr. Opin. Plant Biol. 26, 127–134.

Heard, E., Martienssen, R.A., 2014. Transgenerational epigenetic inheritance: myths and mechanisms. Cell 157, 95–109.

Heger, A., Webber, C., Goodson, M., Ponting, C.P., Lunter, G., 2013. GAT: a simulation framework for testing the association of genomic intervals. Bioinformatics 29, 2046–2048.

Ibarra, C.A., Feng, X., Schoft, V.K., Hsieh, T.-F., Uzawa, R., Rodrigues, J.A., Zemach, A., Chumak, N., Machlicova, A., Nishimura, T., Rojas, D., Fischer, R.L., Tamaru, H., Zilberman, D., 2012. Active DNA demethylation in plant companion cells reinforces transposon methylation in gametes. Science 337, 1360–1364.

Iguchi-Ariga, S.M., Schaffner, W., 1989. CpG methylation of the cAMP-responsive enhancer/promoter sequence TGACGTCA abolishes specific factor binding as well as transcriptional activation. Genes Dev. 3, 612–619.

Jones, J.D.G., Vance, R.E., Dangl, J.L., 2016. Intracellular innate immune surveillance devices in plants and animals. Science 354.

Kawakatsu, T., Nery, J.R., Castanon, R., Ecker, J.R., 2017. Dynamic DNA methylation reconfiguration during seed development and germination. Genome Biol. 18, 171.

Kim, D., Pertea, G., Trapnell, C., Pimentel, H., Kelley, R., Salzberg, S.L., 2013. TopHat2: accurate alignment of transcriptomes in the presence of insertions, deletions and gene fusions. Genome Biol. 14, R36.

Kim, J.-S., Lim, J.Y., Shin, H., Kim, B.-G., Yoo, S.-D., Kim, W.T., Huh, J.H., 2019. ROS1-Dependent DNA Demethylation Is Required for ABA-Inducible NIC3 Expression. Plant Physiol. 179, 1810–1821.

Kong, W., Xia, X., Wang, Q., Liu, L.-W., Zhang, S., Ding, L., Liu, A., La, H., 2020. Impact of DNA Demethylases on the DNA Methylation and Transcription of Arabidopsis *NLR* Genes. Front Genet 11, 460.

Krueger, F., Andrews, S.R., 2011. Bismark: a flexible aligner and methylation caller for Bisulfite-Seq applications. Bioinformatics 27, 1571–1572.

Lahmy, S., Pontier, D., Bies-Etheve, N., Laudié, M., Feng, S., Jobet, E., Hale, C.J., Cooke, R., Hakimi, M.-A., Angelov, D., Jacobsen, S.E., Lagrange, T., 2016. Evidence for ARGONAUTE4-DNA interactions in RNA-directed DNA methylation in plants. Genes Dev. 30, 2565–2570.

Lang, Z., Wang, Y., Tang, K., Tang, D., Datsenka, T., Cheng, J., Zhang, Y., Handa, A.K., Zhu, J.-K., 2017. Critical roles of DNA demethylation in the activation of ripening-induced genes and inhibition of ripening-repressed genes in tomato fruit. Proc. Natl. Acad. Sci. U.S.A. 114, E4511–E4519.

Langmead, B., Trapnell, C., Pop, M., Salzberg, S.L., 2009. Ultrafast and memory-efficient alignment of short DNA sequences to the human genome. Genome Biol. 10, R25.

Le, T.-N., Schumann, U., Smith, N.A., Tiwari, S., Au, P.C.K., Zhu, Q.-H., Taylor, J.M., Kazan, K., Llewellyn, D.J., Zhang, R., Dennis, E.S., Wang, M.-B., 2014. DNA demethylases target promoter transposable elements to positively regulate stress responsive genes in Arabidopsis. Genome Biol. 15, 458.

Li, J., Yang, D.-L., Huang, H., Zhang, G., He, L., Pang, J., Lozano-Durán, R., Lang, Z., Zhu, J.-K., 2020. Epigenetic memory marks determine epiallele stability at loci targeted by de novo DNA methylation. Nat Plants 6, 661–674.

López, A., Ramírez, V., García-Andrade, J., Flors, V., Vera, P., 2011. The RNA silencing enzyme RNA polymerase V is required for plant immunity. PLoS Genet. 7, e1002434.

López Sánchez, A., Stassen, J.H.M., Furci, L., Smith, L.M., Ton, J., 2016. The role of DNA (de)methylation in immune responsiveness of Arabidopsis. Plant J. 88, 361–374.

Matzke, M.A., Mosher, R.A., 2014. RNA-directed DNA methylation: an epigenetic pathway of increasing complexity. Nat. Rev. Genet. 15, 394–408.

Mok, Y.G., Uzawa, R., Lee, J., Weiner, G.M., Eichman, B.F., Fischer, R.L., Huh, J.H., 2010. Domain structure of the DEMETER 5-methylcytosine DNA glycosylase. Proc. Natl. Acad. Sci. U.S.A. 107, 19225–19230.

Monteiro, F., Nishimura, M.T., 2018. Structural, Functional, and Genomic Diversity of Plant NLR Proteins: An Evolved Resource for Rational Engineering of Plant Immunity. Annu Rev Phytopathol 56, 243–267.

Navarro, L., Zipfel, C., Rowland, O., Keller, I., Robatzek, S., Boller, T., Jones, J.D.G., 2004. The transcriptional innate immune response to flg22. Interplay and overlap with Avr gene-dependent defense responses and bacterial pathogenesis. Plant Physiol. 135, 1113–1128.

Navarro, L., Jay F., Nomura, K., He S-H., Voinnet O., 2008. Suppression of the microRNA pathway by bacterial effector proteins. Science 321, 964-967.

Nishimura, M.T., Anderson, R.G., Cherkis, K.A., Law, T.F., Liu, Q.L., Machius, M., Nimchuk, Z.L., Yang, L., Chung, E.-H., El Kasmi, F., Hyunh, M., Osborne Nishimura, E., Sondek, J.E., Dangl, J.L., 2017. TIR-only protein RBA1 recognizes a pathogen effector to regulate cell death in Arabidopsis. Proc. Natl. Acad. Sci. U.S.A. 114, E2053–E2062.

Oldroyd, G.E., Staskawicz, B.J., 1998. Genetically engineered broad-spectrum disease resistance in tomato. Proc. Natl. Acad. Sci. U.S.A. 95, 10300–10305.

O'Malley, R.C., Huang, S.-S.C., Song, L., Lewsey, M.G., Bartlett, A., Nery, J.R., Galli, M., Gallavotti, A., Ecker, J.R., 2016. Cistrome and Epicistrome Features Shape the Regulatory DNA Landscape. Cell 166, 1598.

Pacis, A., Mailhot-Léonard, F., Tailleux, L., Randolph, H.E., Yotova, V., Dumaine, A., Grenier, J.-C., Barreiro, L.B., 2019. Gene activation precedes DNA demethylation in response to infection in human dendritic cells. Proc. Natl. Acad. Sci. U.S.A. 116, 6938–6943.

Pacis, A., Tailleux, L., Morin, A.M., Lambourne, J., MacIsaac, J.L., Yotova, V., Dumaine, A., Danckaert, A., Luca, F., Grenier, J.-C., Hansen, K.D., Gicquel, B., Yu, M., Pai, A., He, C., Tung, J., Pastinen, T., Kobor, M.S., Pique-Regi, R., Gilad, Y., Barreiro, L.B., 2015. Bacterial infection remodels the DNA methylation landscape of human dendritic cells. Genome Res. 25, 1801–1811.

Panda, K., McCue, A.D., Slotkin, R.K., 2020. Arabidopsis RNA Polymerase IV generates 21-22 nucleotide small RNAs that can participate in RNA-directed DNA methylation and may regulate genes. Philos. Trans. R. Soc. Lond., B, Biol. Sci. 375, 20190417.

Pavet, V., Quintero, C., Cecchini, N.M., Rosa, A.L., Alvarez, M.E., 2006. Arabidopsis displays centromeric DNA hypomethylation and cytological alterations of heterochromatin upon attack by *Pseudomonas syringae*. Mol. Plant Microbe Interact. 19, 577–587.

902 Penterman, J., Zilberman, D., Huh, J.H., Ballinger, T., Henikoff, S., Fischer, R.L., 2007. DNA demethylation in
903 the Arabidopsis genome. PNAS 104, 6752–6757.
904
905 Qi, Y., He, X., Wang, X.-J., Kohany, O., Jurka, J., Hannon, G.J., 2006. Distinct catalytic and non-catalytic roles
906 of ARGONAUTE4 in RNA-directed DNA methylation. Nature 443, 1008–1012.
907
908 Qian, W., Miki, D., Zhang, H., Liu, Y., Zhang, X., Tang, K., Kan, Y., La, H., Li, X., Li, S., Zhu, X., Shi, X.,
909 Zhang, K., Pontes, O., Chen, X., Liu, R., Gong, Z., Zhu, J.-K., 2012. A histone acetyltransferase regulates active
910 DNA demethylation in Arabidopsis. Science 336, 1445–1448.
911
912 Ramírez, F., Ryan, D.P., Grüning, B., Bhardwaj, V., Kilpert, F., Richter, A.S., Heyne, S., Dündar, F., Manke, T.,
913 2016. deepTools2: a next generation web server for deep-sequencing data analysis. Nucleic Acids Res. 44, W160-
914 165.
915
916 Roth, C., Lüdke, D., Klenke, M., Quathamer, A., Valerius, O., Braus, G.H., Wiermer, M., 2017. The truncated
917 NLR protein TIR-NBS13 is a MOS6/IMPORTIN-α3 interaction partner required for plant immunity. Plant J. 92,
918 808–821.
919
920 Schübeler, D., 2015. Function and information content of DNA methylation. Nature 517, 321–326.
921
922 Schumann, U., Lee, J.M., Smith, N.A., Zhong, C., Zhu, J.-K., Dennis, E.S., Millar, A.A., Wang, M.-B., 2019.
923 DEMETER plays a role in DNA demethylation and disease response in somatic tissues of Arabidopsis. Epigenetics
924 14, 1074–1087.
925
926 Shen, Q.-H., Saijo, Y., Mauch, S., Biskup, C., Bieri, S., Keller, B., Seki, H., Ulker, B., Somssich, I.E., Schulze-
927 Lefert, P., 2007. Nuclear activity of MLA immune receptors links isolate-specific and basal disease-resistance
928 responses. Science 315, 1098–1103.
929
930 Steidele, C., Stam, R., 2020. Multi-omics approach highlights differences between functional RLP classes in
931 *Arabidopsis thaliana*. bioRxiv 2020.08.07.240911.
932
933 Stroud, H., Do, T., Du, J., Zhong, X., Feng, S., Johnson, L., Patel, D.J., Jacobsen, S.E., 2014. Non-CG methylation
934 patterns shape the epigenetic landscape in Arabidopsis. Nat. Struct. Mol. Biol. 21, 64–72.
935
936 Swiderski, M.R., Birker, D., Jones, J.D.G., 2009. The TIR domain of TIR-NB-LRR resistance proteins is a
937 signaling domain involved in cell death induction. Mol. Plant Microbe Interact. 22, 157–165.
938
939 Tang, K., Lang, Z., Zhang, H., Zhu, J.-K., 2016. The DNA demethylase ROS1 targets genomic regions with
940 distinct chromatin modifications. Nat Plants 2, 16169.
941
942 Tate, P.H., Bird, A.P., 1993. Effects of DNA methylation on DNA-binding proteins and gene expression. Curr.
943 Opin. Genet. Dev. 3, 226–231.
944
945 Thomma, B.P.H.J., Nürnberger, T., Joosten, M.H.A.J., 2011. Of PAMPs and effectors: the blurred PTI-ETI
946 dichotomy. Plant Cell 23, 4–15.
947
948 van Wersch, S., Tian, L., Hoy, R., Li, X., 2020. Plant NLRs: The Whistleblowers of Plant Immunity. Plant
949 Communications 1, 100016.
950
951 Walker, J., Gao, H., Zhang, J., Aldridge, B., Vickers, M., Higgins, J.D., Feng, X., 2018. Sexual-lineage-specific
952 DNA methylation regulates meiosis in Arabidopsis. Nat. Genet. 50, 130–137.
953
954 Watt, F., Molloy, P.L., 1988. Cytosine methylation prevents binding to DNA of a HeLa cell transcription factor
955 required for optimal expression of the adenovirus major late promoter. Genes Dev. 2, 1136–1143.
956
957 Wei, H.-L., Chakravarthy, S., Mathieu, J., Helmann, T.C., Stodghill, P., Swingle, B., Martin, G.B., Collmer, A.,
958 2015. *Pseudomonas syringae* pv. *tomato* DC3000 Type III Secretion Effector Polymutants Reveal an Interplay
959 between HopAD1 and AvrPtoB. Cell Host Microbe 17, 752–762.
960
961 Weigel, D., Colot, V., 2012. Epialleles in plant evolution. Genome Biol. 13, 249.

962 Wierzbicki, A.T., Ream, T.S., Haag, J.R., Pikaard, C.S., 2009. RNA polymerase V transcription guides
963 ARGONAUTE4 to chromatin. Nat. Genet. 41, 630–634.
964
965 Xie, Z., Johansen, L.K., Gustafson, A.M., Kasschau, K.D., Lellis, A.D., Zilberman, D., Jacobsen, S.E., Carrington,
966 J.C., 2004. Genetic and functional diversification of small RNA pathways in plants. PLoS Biol. 2, E104.
967
968 Yamamuro, C., Miki, D., Zheng, Z., Ma, J., Wang, J., Yang, Z., Dong, J., Zhu, J.-K., 2014. Overproduction of
969 stomatal lineage cells in Arabidopsis mutants defective in active DNA demethylation. Nat Commun 5, 4062.
970
971 Yang, D.-L., Zhang, G., Tang, K., Li, J., Yang, L., Huang, H., Zhang, H., Zhu, J.-K., 2016. Dicer-independent
972 RNA-directed DNA methylation in Arabidopsis. Cell Res. 26, 66–82.
973
974 Yin, Y., Morgunova, E., Jolma, A., Kaasinen, E., Sahu, B., Khund-Sayeed, S., Das, P.K., Kivioja, T., Dave, K.,
975 Zhong, F., Nitta, K.R., Taipale, M., Popov, A., Ginno, P.A., Domcke, S., Yan, J., Schübeler, D., Vinson, C.,
976 Taipale, J., 2017. Impact of cytosine methylation on DNA binding specificities of human transcription factors.
977 Science 356.
978
979 Yu, A., Lepère, G., Jay, F., Wang, J., Bapaume, L., Wang, Y., Abraham, A.-L., Penterman, J., Fischer, R.L.,
980 Voinnet, O., Navarro, L., 2013. Dynamics and biological relevance of DNA demethylation in Arabidopsis
981 antibacterial defense. Proc. Natl. Acad. Sci. U.S.A. 110, 2389–2394.
982
983 Zervudacki, J., Yu, A., Amesefe, D., Wang, J., Drouaud, J., Navarro, L., Deleris, A., 2018. Transcriptional control
984 and exploitation of an immune-responsive family of plant retrotransposons. EMBO J. 37.
985
986 Zhai, J., Bischof, S., Wang, H., Feng, S., Lee, T.-F., Teng, C., Chen, X., Park, S.Y., Liu, L., Gallego-Bartolome,
987 J., Liu, W., Henderson, I.R., Meyers, B.C., Ausin, I., Jacobsen, S.E., 2015. A One Precursor One siRNA Model
988 for Pol IV-Dependent siRNA Biogenesis. Cell 163, 445–455.
989
990 Zhang, H., Lang, Z., Zhu, J.-K., 2018. Dynamics and function of DNA methylation in plants. Nature Reviews
991 Molecular Cell Biology 19, 489–506.
992
993 Zhang, Y., Dorey, S., Swiderski, M., Jones, J.D.G., 2004. Expression of RPS4 in tobacco induces an AvrRps4-
994 independent HR that requires EDS1, SGT1 and HSP90. Plant J. 40, 213–224.
995
996 Zilberman, D., Cao, X., Johansen, L.K., Xie, Z., Carrington, J.C., Jacobsen, S.E., 2004. Role of Arabidopsis
997 ARGONAUTE4 in RNA-directed DNA methylation triggered by inverted repeats. Curr. Biol. 14, 1214–1220.
998
999 Zipfel, C., Robatzek, S., Navarro, L., Oakeley, E.J., Jones, J.D.G., Felix, G., Boller, T., 2004. Bacterial disease
1000 resistance in Arabidopsis through flagellin perception. Nature 428, 764–767.

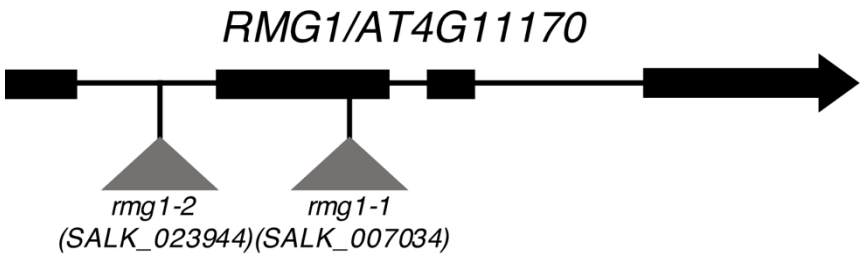

Supplemental Figure 1. Scheme representing T-DNA insertion sites in *rmg1-1* and *rmg1-2* mutant lines. T-DNA insertions in *rmg1-1* (SALK_007034) and *rmg1-2* (SALK_023944) are located in the second exon and in the first intron of *RMG1*, respectively.

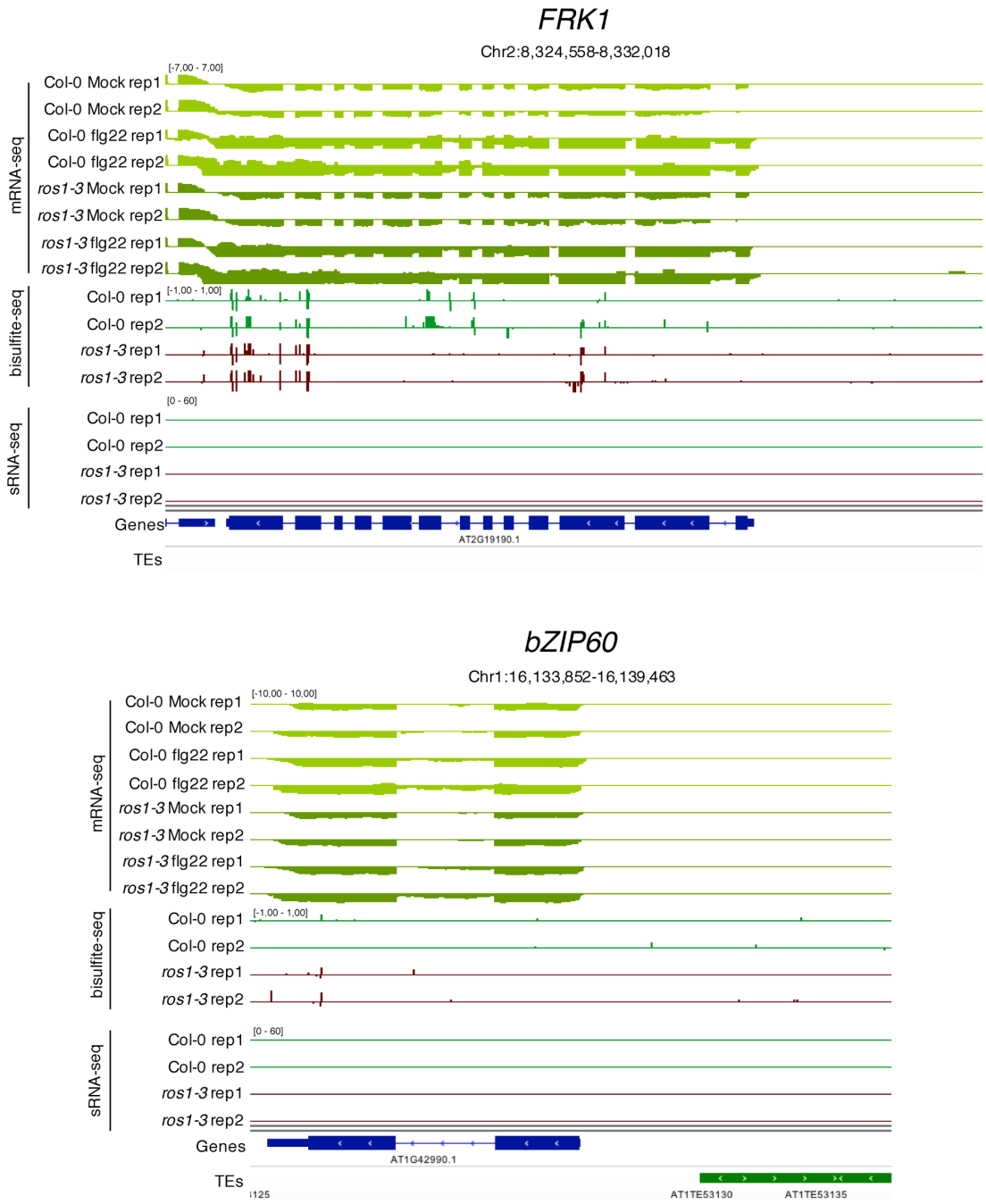

Supplemental Figure 2. *FRK1* and *bZIP60* promoters are not hypermethylated in *ros1-3* mutants.
IGV snapshots showing mRNA levels (mRNA-seq) after syringe-infiltration of mock (water) or 1 μM of flg22 peptide for Col-0 and *ros1-3*, and cytosine methylation levels (Bs-Seq) and siRNA levels (sRNA-seq) in 5-week-old untreated rosette leaves of Col-0 and *ros1-3,* at the *Flg22-induced Receptor-like Kinase 1* (*FRK1*) (upper panel) and *bZIP60* (lower panel) loci.

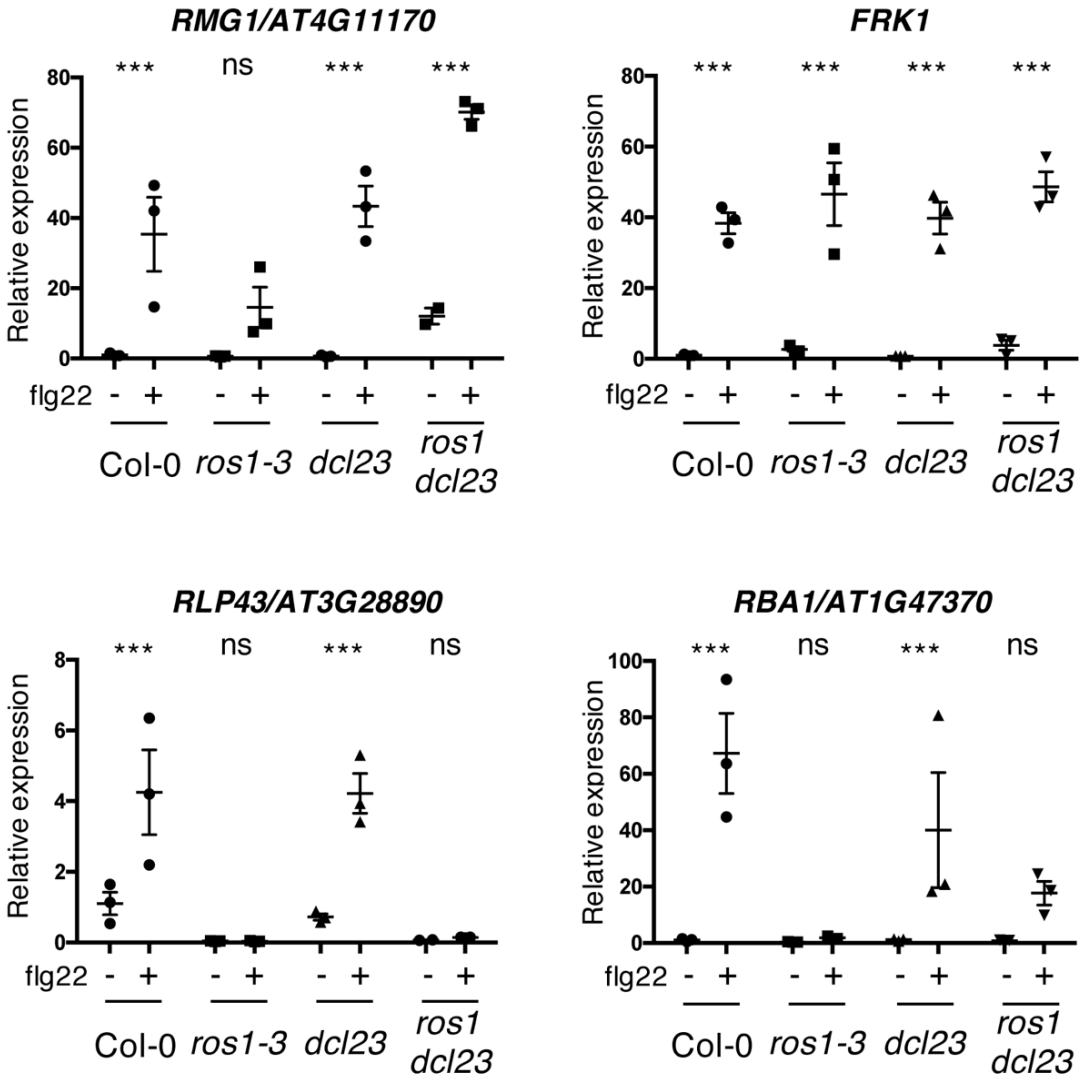

Supplemental Figure 3. The flg22-triggered induction of *RMG1* and *RBA1* is restored, while *RLP43* remains in a repressed state in the *ros1dcl23*-elicited mutant.

Second biological replicate of RT-qPCR analyses depicting *RMG1*, *FRK1, RLP43* and *RBA1* mRNA levels in 5-week-old rosette leaves of Col-0, *ros1-3*, *dcl23* and *ros1dcl23* treated with either mock (water) or 1 μM of flg22 for 6h. The mRNA levels are relative to the level of *UBQ* transcripts. Statistical significance of flg22 treatment on expression was assessed using a two-way ANOVA test and a Sidak's multiple comparisons test.

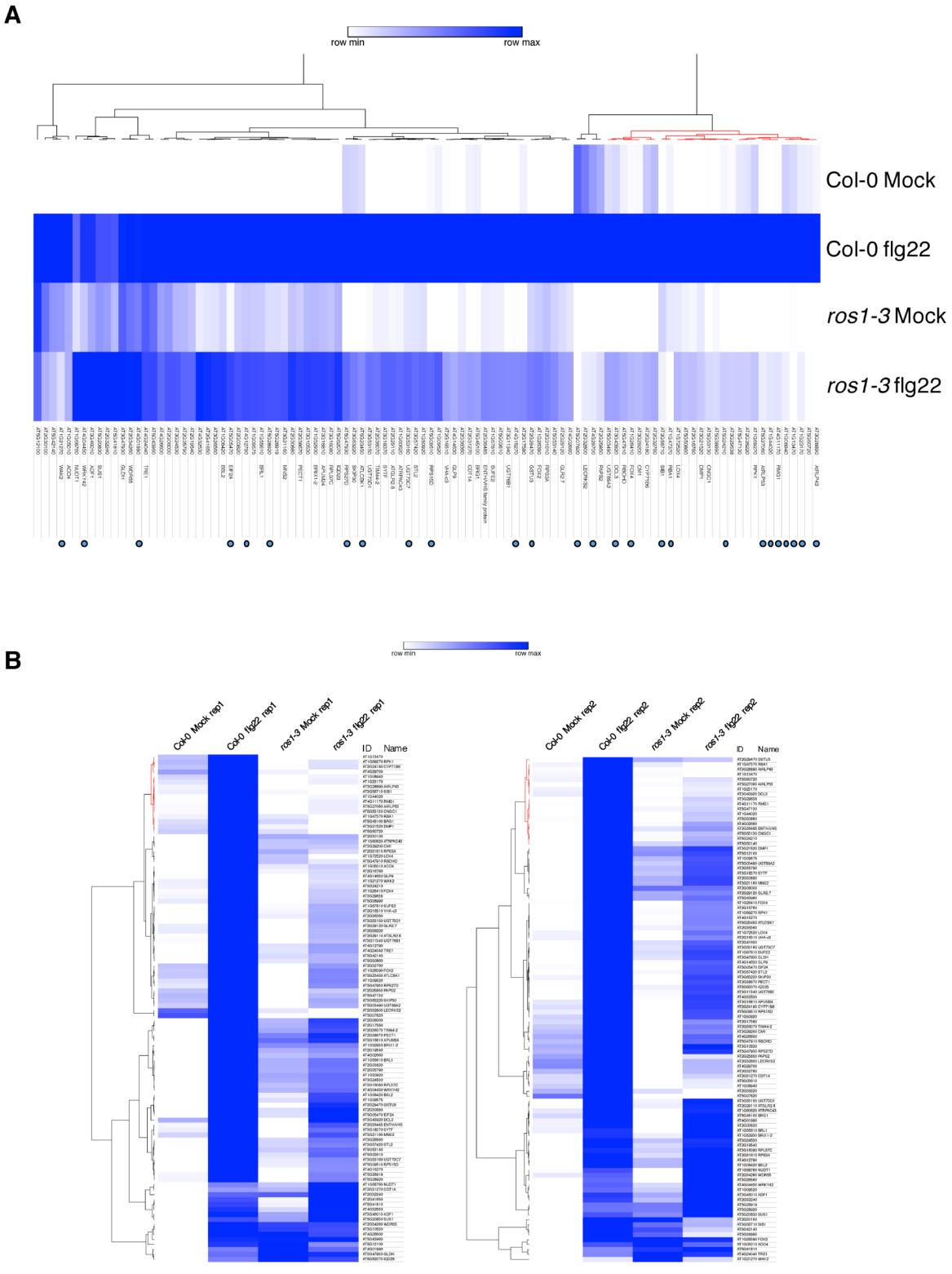

Supplemental Figure 4. RNA sequencing experiment in 5-week-old rosette leaves of Col-0 and *ros1-3* syringe-infiltrated with either mock or flg22 for 6h.

A. Heatmap representing the relative expression of the 102 less-induced genes in Col-0 and *ros1-3* mutants upon 6h of mock or flg22 treatments. AGI numbers and gene names are shown for all individual gene. Merged data from two independent biological replicates are presented.

B. Heatmaps showing the relative expression of the 102 less-induced genes for each independent biological replicate.

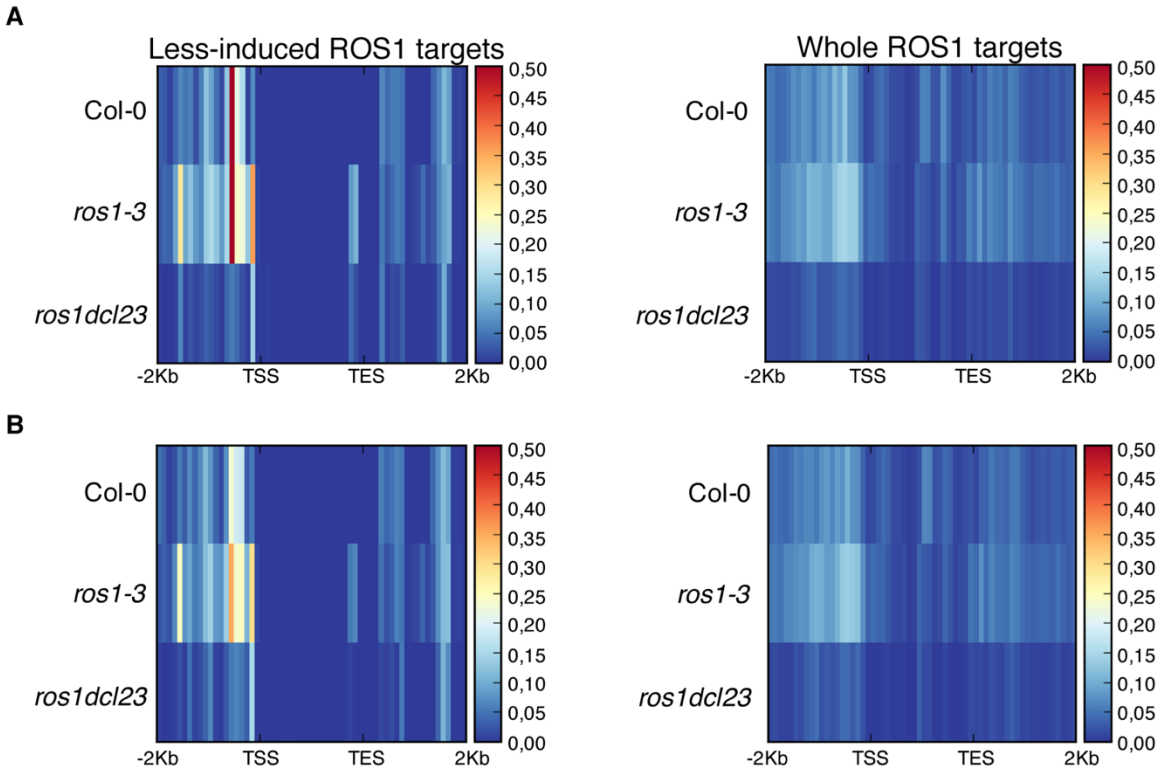

Supplemental Figure 5. Analysis of 23-24 nt siRNA levels for the groups of 102 less-induced genes and 2943 genes carrying hyperDMRs in the *ros1-3* mutant background.

A. Heatmaps representing 23nt- and 24nt-long siRNA levels at the 102 less-induced genes (left panel) and at the 2943 genes presenting hyperDMR in *ros1-3* (right panel) on replicate 1. Global siRNA levels were quantified from 2Kb upstream sequence from the transcription start site (TSS), the gene body, and 2 Kb downstream sequence of the transcription end site (TES) of genes in 5-week-old rosette leaves in non-treated Col-0*, ros1-3* and *ros1dcl23*.

B. Heatmaps representing 23nt- and 24nt-long siRNA levels at the 102 less-induced genes (left panel) and at the 2943 genes presenting hyperDMR in *ros1-3* (right panel) on replicate 2. Global siRNA levels were quantified from 2Kb upstream sequence from the transcription start site (TSS), the gene body, and 2 Kb downstream sequence of the transcription end site (TES) of genes in 5-week-old rosette leaves in non-treated Col-0*, ros1-3* and *ros1dcl23*.

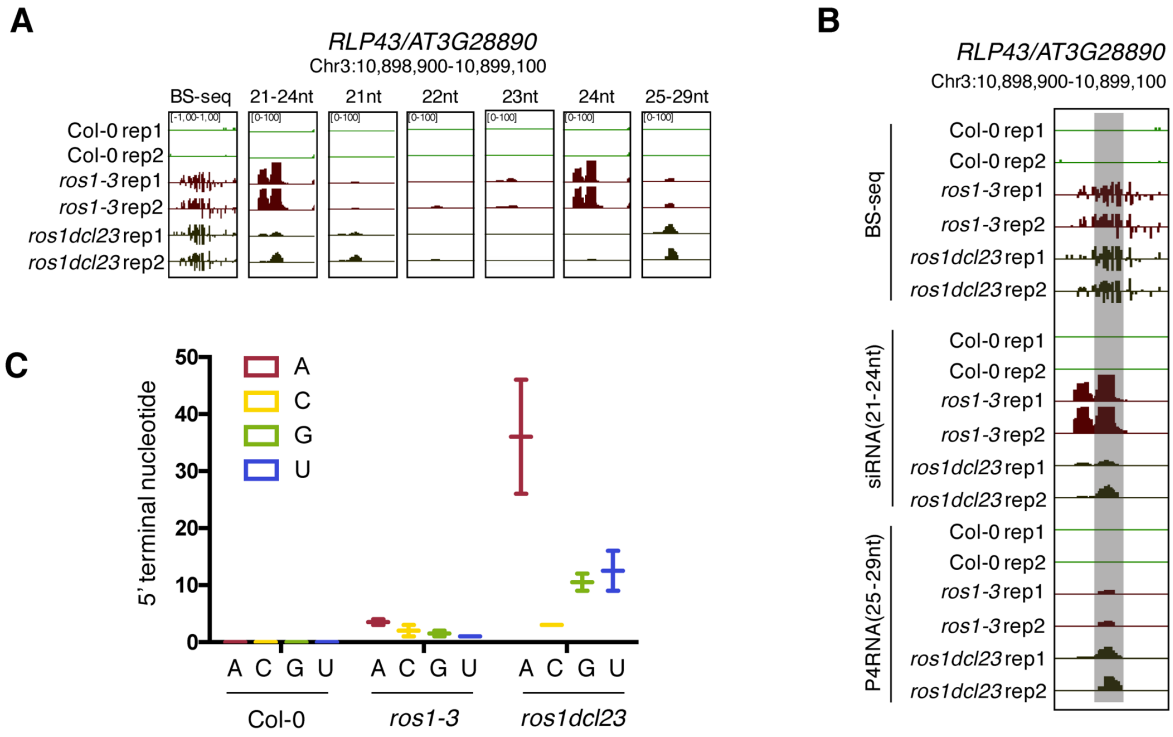

Supplemental Figure 6. Gain of 21-nt siRNA and P4RNAs at the *RLP43* promoter in the *ros1dcl23* background might contribute to the maintenance of DNA methylation levels in this triple mutant.

A. Snapshot representing levels of DNA methylation and siRNA species classified per size at the *RLP43* promoter, in 5-week-old rosette leaves of untreated Col-0, *ros1-3* and *ros1dcl23*.

B. Snapshot representing levels of DNA methylation, 21-24 nt siRNAs and 25-29 nt P4RNAs at the *RLP43* promoter, in 5-week-old rosette leaves of untreated Col-0, *ros1-3* and *ros1dcl23*. The region presenting increased P4RNAs is highlighted in the grey box.

C. Number of putative P4RNAs classified depending on the nucleotide present at the 5' terminal in Col-0, *ros1-3* and *ros1dcl23*. Data from the two biological replicates are presented.

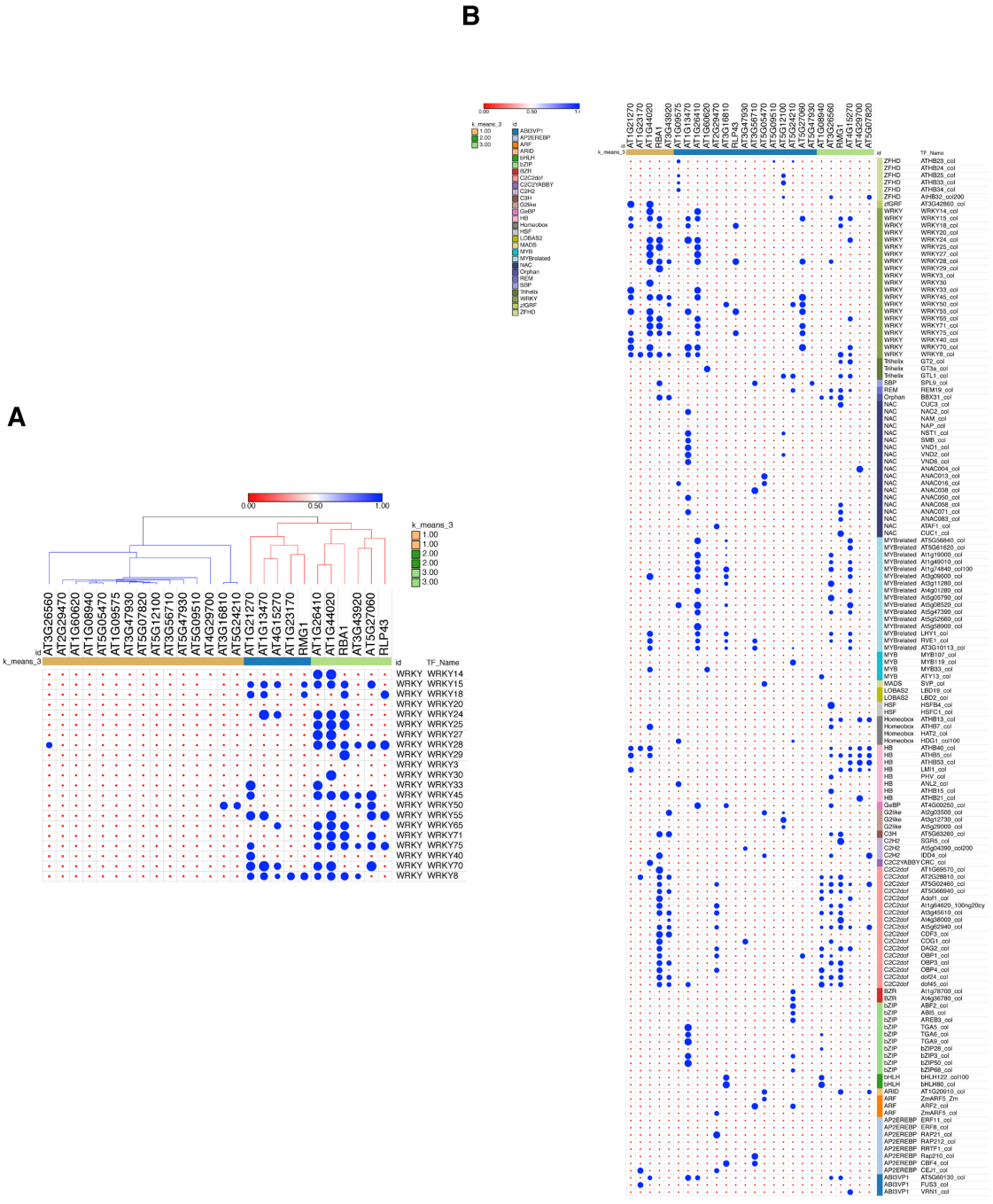

Supplemental Figure 7. GAT analysis of all the transcription factor classes binding to the 26 stringent ROS1 target promoters.

A. GAT analysis performed on publicly available DAP-sequencing data (O'Malley et al., 2016) for WRKY transcription factors at the 26 stringent ROS1 primary targets. This analysis was conducted on 26 stringent less-induced ROS1 targets, from which promoter hyperDMR sequences exhibiting dense methylated levels in *ros1-3* mutants were manually selected (these genes are represented by blue dots in Supplementary Figure 4).

B. GAT analysis performed on publicly available DAP-seq data (O'Malley et al., 2016) identified transcription factors with significant enrichment at the promoter demethylated regions from the 26 stringent less-induced ROS1 targets.

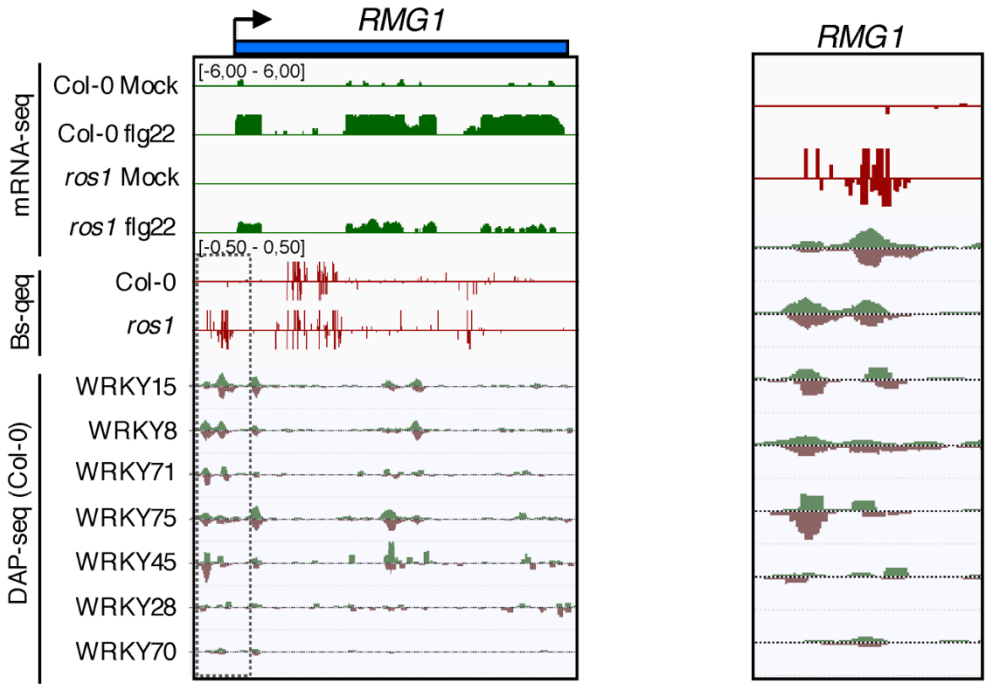

Supplemental Figure 8. WRKY DNA binding peaks are present at the *RMG1* promoter region that is subjected to ROS1-directed demethylation.
Snapshots representing, from top to bottom, RNA-seq, BS-seq and DAP-seq datasets at the *RMG1* locus (left panel) with an enlargement surrounding the hyperDMR and the WRKY-binding peaks (right panel).

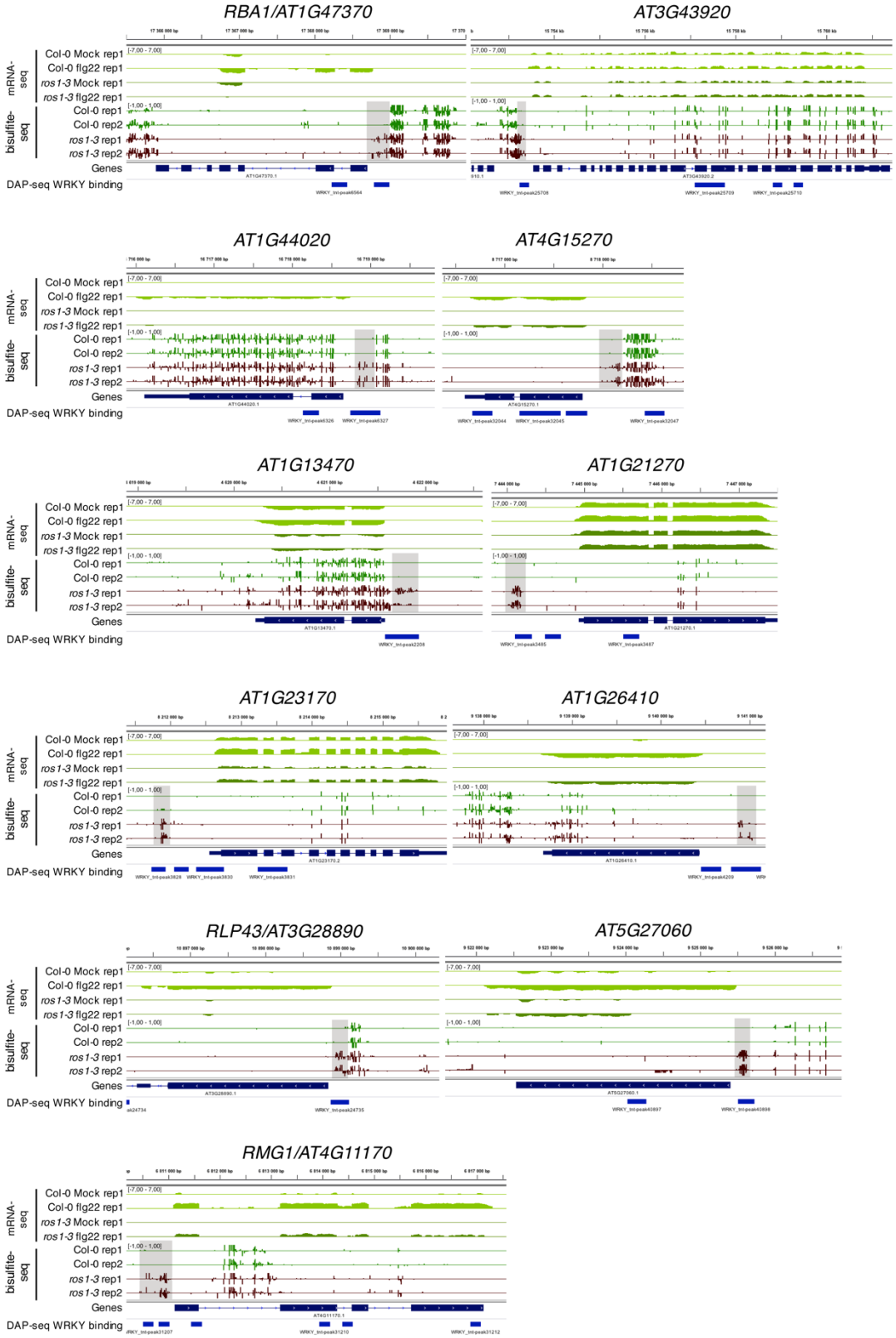

Supplemental Figure 9. Position of WRKY DNA binding peaks at the 11 flg22-induced ROS1 targets. Snapshots depicting RNA-seq (rep1), BS-seq (rep1 and rep2) and the position of WRKY-binding sites observed in the DAP-seq data (O'Malley et al., 2016) in Col-0 and *ros1-3* untreated rosette leaves.

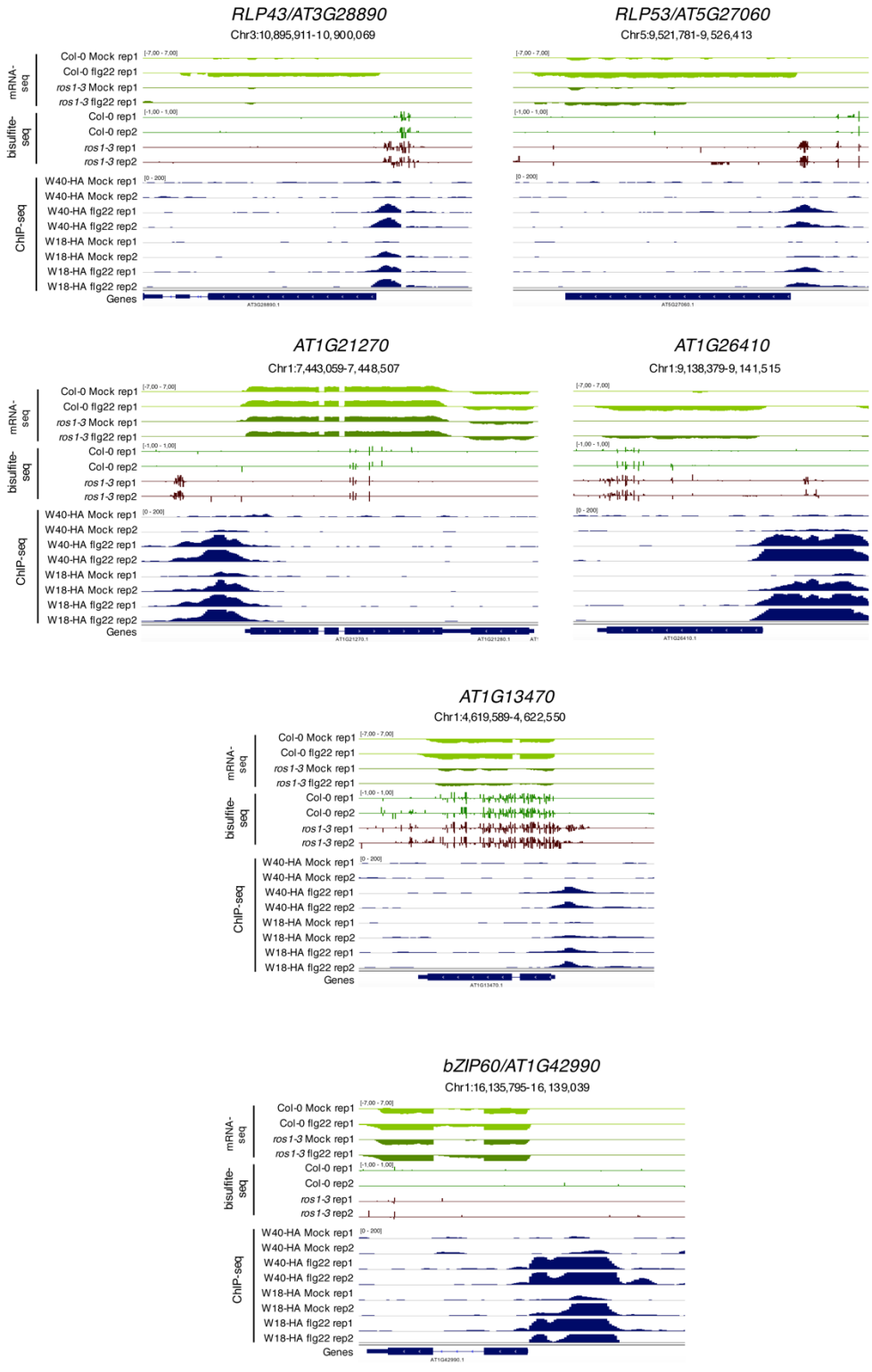

Supplemental Figure 10. Flg22-triggered chromatin association of WRKY18-HA and WRKY40-HA at the promoters of 5 less-induced ROS1 targets and at the promoter of the positive control bZIP60.
Snapshots representing mRNA-seq and BS-seq of Col-0 and *ros1* untreated rosette leaves and ChIP-seq data for *wrky18* WRKY18-HA and *wrky40* WRKY40-HA seedlings subjected to either mock (medium without flg22) or flg22 (medium supplemented with flg22) for 2h, at *RLP43*, *RLP53/AT5G27060*, *AT1G21270*, *AT1G26410*, *AT1G13470* and *bZIP60* (Birkenbihl et al., 2017).

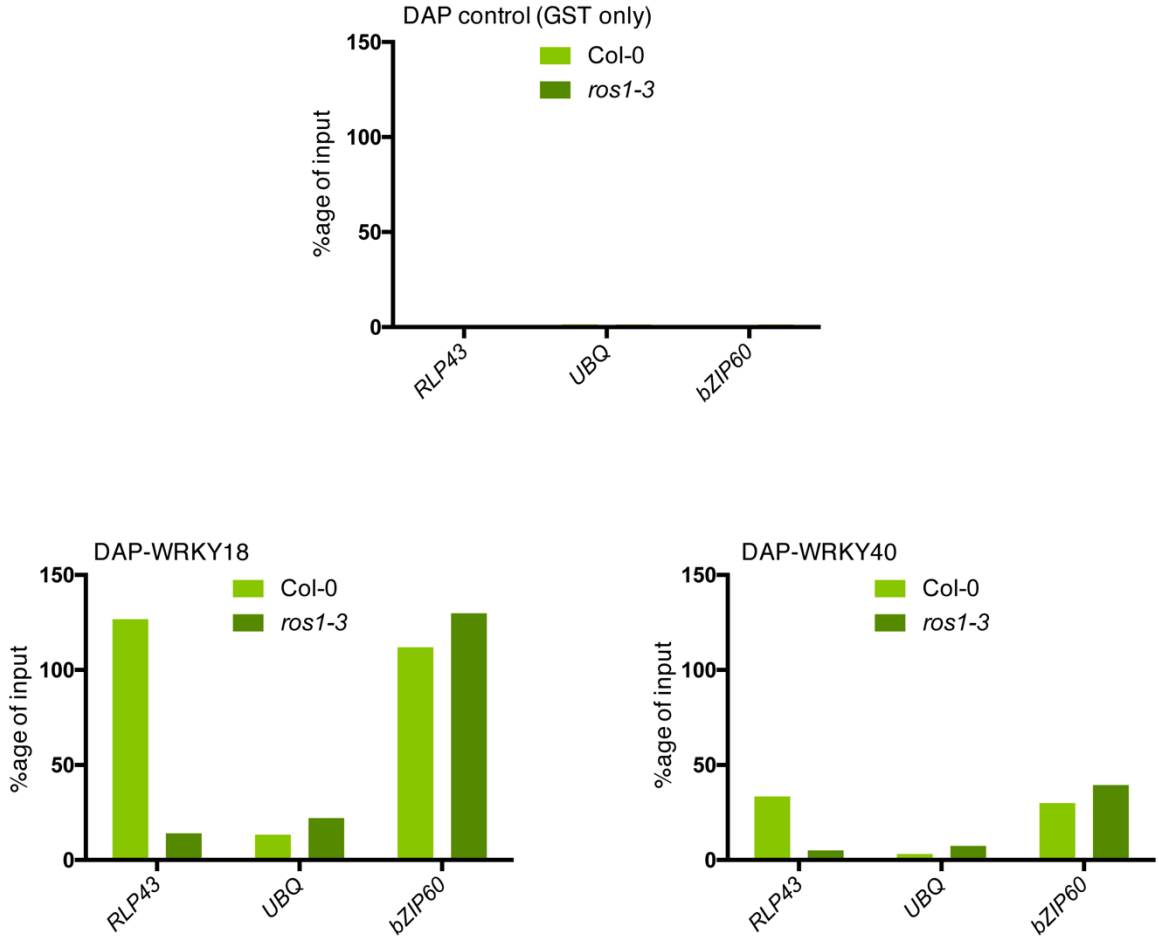

Supplemental Figure 11. ROS1-directed demethylation is crucial for the binding of WRKY18 and WRKY40 at the *RLP43* promoter.

The ability of WRKY18 and WRKY40 to bind DNA corresponding to the demethylated region of the *RLP43* promoter is abolished in the *ros1-3* mutant background. Second replicate of the DAP-qPCR analysis at the *RLP43* promoter upon pull-down of Col-0 or *ros1-3* genomic DNA by GST (negative control) (upper panel), WRKY18-GST (left panel) or WRKY40-GST (right panel). UBQ and *bZIP60* served as negative and positive controls, respectively.

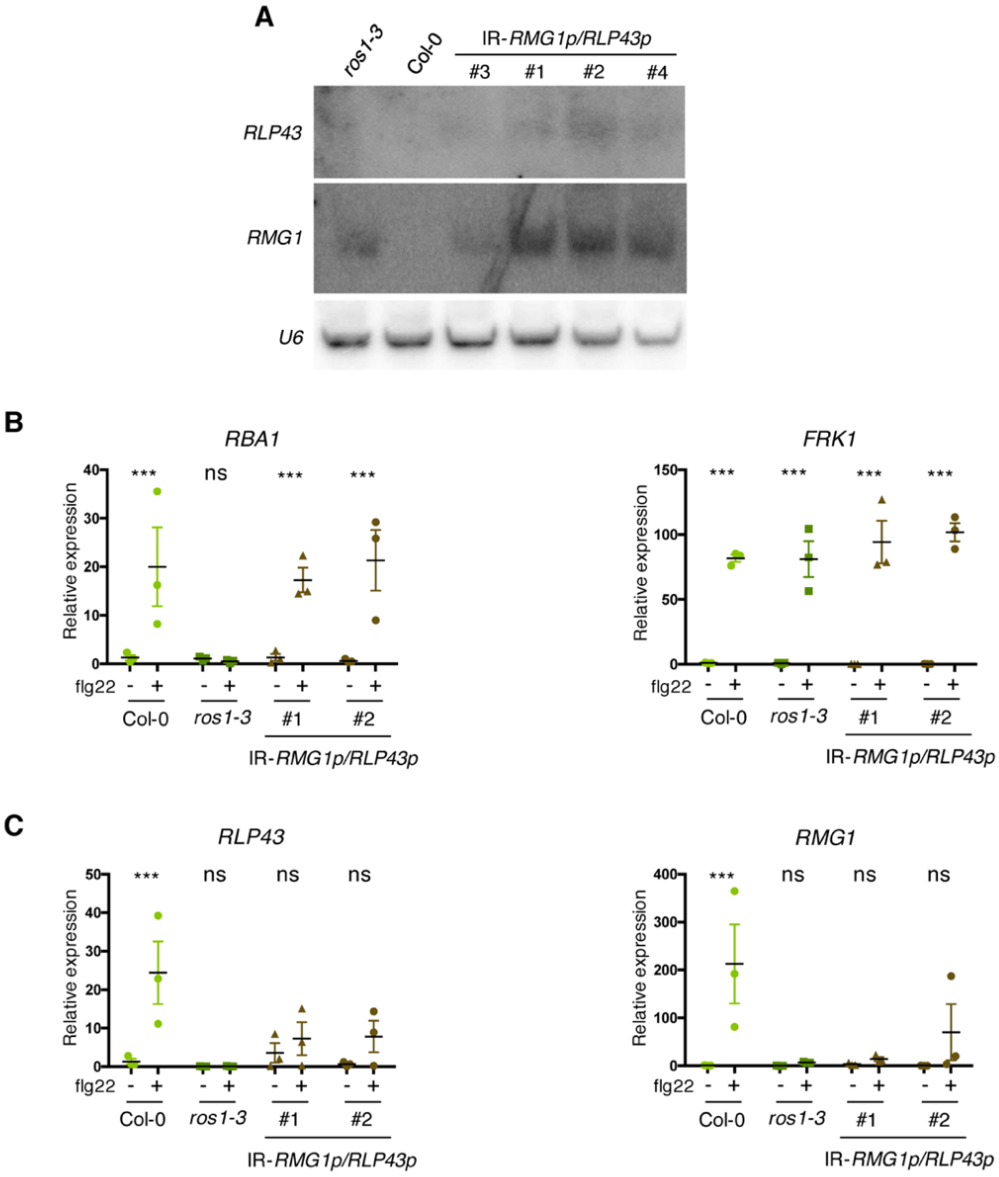

Supplemental Figure 12. Artificial siRNA-directed remethylation of *RMG1* and *RLP43* promoters in the Col-0 background limits flg22-triggered induction of these genes.

A. Accumulation of siRNAs at *RLP43* and *RMG1* promoters in IR-*RMG1p/RLP43p* lines were detected by low molecular weight Northern blot analysis. U6 was used as a loading control.

B. Result from another independent experiment showing gene expression of *RBA1* and *FRK1* upon 6h mock or flg22 treatment. RT-qPCR analyses of mRNAs from these genes were performed in Col-0, *ros1-3* and the two IR-*RMG1p/RLP43p* independent transgenic lines treated with either mock (water) or 1 μM of flg22 for 6h. The mRNA levels are relative to the level of *UBQ* transcripts. Statistical significance of flg22 treatment on expression was assessed using a two-way ANOVA test and a Sidak's multiple comparisons test.

C. Result from another independent experiment showing gene expression of *RLP43* and *RMG1* upon 6h mock or flg22 treatment. RT-qPCR analyses of mRNAs from these genes were performed in Col-0, *ros1-3* and the two IR-*RMG1p/RLP43p* independent transgenic lines treated with either mock (water) or 1 μM of flg22 for 6h. The mRNA levels are relative to the level of *UBQ* transcripts. Statistical significance of flg22 treatment on expression was assessed using a two-way ANOVA test and a Sidak's multiple comparisons test.

Primer name	Primer sequence
RT-qPCR	
RMG1-F	GGGCTAAGCTATCTACCGCA
RMG1-R	TTCTAAGCGGCTGAACTCCA
RLP43-F	CAATTTTCGGACGTGCTTGC
RLP43-R	GCAGCTTAGGTCTAGCTCGA
RBA1-F1	CGCTTGCTCAAAAGTCTCGA
RBA1-R1	TCTTCTGTGTCCTCGCTTGT
FRK1-F	TATCTTGAGCTGGGAAGAGAGG
FRK1-R	AGTCGAATAGTACTCGGGGTCA
GUS-F	ACCTCTTTAGGCATTGGTTTCG
GUS-R	TCACGCGCTATCAGCTCTTTAATC
UBQ-F	GGGCTTTCTCATTGTTGGTC
UBQ-R	TGAAGTCGTGAGACAGCGTTG
DAP-qPCR	
RLP43-F	ACAAGTCGCCACGTCATTAGA
RLP43-R	TCTGGAAATTGTGATGGTACGT
bZIP60-F	GTTGCCTCCTACGTCCAGAA
bZIP60-R	CCTAGGCCTCGAACCCTTAC
UBQ-F	GGGCTTTCTCATTGTTGGTC
UBQ-R	TGAAGTCGTGAGACAGCGTTG
McrBC	
RLP43-F	ACAAGTCGCCACGTCATTAGA
RLP43-R	TCTGGAAATTGTGATGGTACGT
RMG1-F	GCAGCAAAAGTCTTTACAGCC
RMG1-R	TGCATCTCATTAAAGGTCGCC
Cloning WRKY18	
WRKY18-F	ATGGACGGTTCTTCGTTTCTCG
WRKY18-R	TGTTCTAGATTGCTCCATTAACC

Supplemental Table 1. List of primers used in this study.